CFD MODELLING OF MULTIPHASE FLOW IN STATIC MIXER

VIKNESVARAN S/O SILVERRAJAN

FACULTY OF ENGINEERING
UNIVERSITY OF MALAYA
KUALA LUMPUR

2020

CFD MODELLING OF MULTIPHASE FLOW IN STATIC MIXER

VIKNESVARAN S/O SILVERRAJAN

PROJECT SUBMITTED IN FULFILMENT OF THE REQUIREMENTS
FOR THE DEGREE OF MASTERS OF
MECHANICAL ENGINEERING

FACULTY OF ENGINEERING
UNIVERSITY OF MALAYA
KUALA LUMPUR

2020

UNIVERSITY OF MALAYA
ORIGINAL LITERARY WORK DECLARATION

Name of Candidate: Viknesvaran s/o Silverrajan

Matric No: KQK180037

Name of Degree: Master of Mechanical Engineering

Title of Research Report : CFD Modelling of Multiphase Flow in Static Mixer

Field of Study: Computational Fluid Dynamic

I do solemnly and sincerely declare that:

(1) I am the sole author/writer of this Work;

(2) This Work is original;

(3) Any use of any work in which copyright exists was done by way of fair dealing and for permitted purposes and any excerpt or extract from, or reference to or reproduction of any copyright work has been disclosed expressly and sufficiently and the title of the Work and its authorship have been acknowledged in this Work;

(4) I do not have any actual knowledge nor do I ought reasonably to know that the making of this work constitutes an infringement of any copyright work;

(5) I hereby assign all and every rights in the copyright to this Work to the University of Malaya ("UM"), who henceforth shall be owner of the copyright in this Work and that any reproduction or use in any form or by any means whatsoever is prohibited without the written consent of UM having been first had and obtained;

(6) I am fully aware that if in the course of making this Work I have infringed any copyright whether intentionally or otherwise, I may be subject to legal action or any other action as may be determined by UM.

Candidate's Signature   Date:

Subscribed and solemnly declared before,

Witness's Signature Date:

Name:

Designation:

CFD MODELLING OF MULTIPHASE FLOW IN STATIC MIXER

Abstract

Modelling of Multiphase flow through a Kenics static mixer were presented in this paper. Multiphase mixing is a challenging process in industries such as pharmaceutical, food and petroleum since two-different phases can be immiscible towards each other. Stirred tank mixing is the most common method used in industries. However, this type of method costs a lot in terms of energy and manpower specially when mixing immiscible liquids. Hence, The Kenics Static Mixer could be a good solution for multiphase mixing when its correctly configured and studied. Two phases used in this paper were aqueous solution: refined CMC as continuous phase and oil: silicon oil 50 as dispersed phase. The first part of this paper is validation of the simulation. For this purpose, a CFD modelling journal selected and compared. After the validation, the same model was used to study the effect of static mixer blade twist angle and length on the pressure drop and mixing efficiency. The modelling involved a static mixer with 10 blades inserted in clockwise and anti-clockwise manner. For the validation purpose, the pressure drop across a blade is compared with the journal and the mixing efficiency is validated by observing the local volume fraction distribution for the dispersed phase. Then, the effect of twisting angle on static mixer performance studied by twisting the blade with angle of 180^0, 150^0, 120^0 and 90^0. And then, the 180^0 blade is used to study the effect of blade length with the variation of 30mm, 33.75mm, 37.5mm, 41.25mm and 45mm. The ansys R3 student version were used to simulate. The validation of pressure drops showed good agreement with the literature for Reynolds number of 100 and 200. The study on mixing performance showed good agreement with the literature eventhough the pattern were not exactly same. This could be due to the limitation of 512K mesh cells in ansys student version and the different meshing technique were applied. The 90^0 degree blade outperform the standard 180^0 degree blade in terms of pressure drop and mixing performance. The pressure drop could be reduced from 15kPa to 9.8kPa. The quantitative analysis of mixing performance showed that 90^0 degree blade had better uniformity index compared to 180^0 degree blade. The length of the blade does not show a significant effect on the pressure drop nor mixing efficiency.

PEMODELAN CFD ALIRAN MULTIFASA DALAM STATIC MIXER

Abstrak

Pemodelan aliran Multifasa melalui pengadun statik Kenics dibentangkan dalam kertas ini. Pencampuran multifasa adalah proses yang mencabar dalam industri seperti farmaseutikal, makanan dan petroleum kerana dua fasa berbeza tidak dapat larut sesama. Pengadukan tangki kacau adalah kaedah yang paling biasa digunakan dalam industri. Walau bagaimanapun, kaedah ini memerlukan tenaga mekanikal dan tenaga manusia terutamanya ketika mencampurkan cecair yang tidak dapat larut sesama. Oleh itu, The Kenics Static Mixer boleh menjadi penyelesaian yang baik untuk pencampuran pelbagai fasa apabila dikonfigurasikan dan dikajikan dengan betul. Dua fasa yang digunakan dalam kertas ini adalah larutan berair: CMC halus sebagai fasa berterusan dan minyak: minyak silikon 50 sebagai fasa tersebar. Bahagian pertama kertas ini adalah pengesahan simulasi. Untuk tujuan ini, jurnal pemodelan CFD dipilih dan dibandingkan. Selepas pengesahan, model yang sama digunakan untuk mengkaji pengaruh sudut putaran bilah pengadun statik dan panjang pada penurunan tekanan dan kecekapan pencampuran. Pemodelan tersebut melibatkan pengadun statik dengan 10 bilah dimasukkan mengikut arah jam dan lawan arah jam. Untuk tujuan pengesahan, penurunan tekanan melintasi bilah dibandingkan dengan jurnal dan kecekapan pencampuran disahkan dengan memerhatikan taburan pecahan isipadu tempatan untuk fasa tersebar. Kemudian, kesan sudut berpusing pada prestasi pengadun statik dikaji dengan memutar pisau dengan sudut 180^0, 150^0, 120^0 dan 90^0. Dan kemudian, bilah 180^0 digunakan untuk mengkaji kesan panjang pisau dengan variasi 30mm, 33.75mm, 37.5mm, 41.25mm dan 45mm. Versi pelajar ansys R3 digunakan untuk membuat simulasi. Pengesahan penurunan tekanan menunjukkan kesepakatan yang baik dengan literatur untuk bilangan Reynolds 100 dan 200. Kajian mengenai prestasi pencampuran menunjukkan persetujuan yang baik dengan literatur walaupun coraknya tidak sama. Ini mungkin disebabkan oleh keterbatasan 512K sel mesh dalam versi pelajar ansys dan teknik meshing yang berbeza diterapkan. Bilah 90^0 darjah mengatasi bilah standard 180^0 darjah dari segi penurunan tekanan dan prestasi pencampuran. Penurunan tekanan dapat dikurangkan dari 15kPa menjadi 9.8kPa. Analisis kuantitatif prestasi pencampuran menunjukkan bahawa pisau 90^0 darjah mempunyai indeks keseragaman yang lebih baik berbanding bilah 180^0 darjah. Panjang bilah tidak menunjukkan kesan yang signifikan terhadap penurunan tekanan atau kecekapan pencampuran.

ACKNOWLEDGEMENTS

I would like to express my gratitude to god/source of creation who never let me down in my worst times. The guidance helping me to survive. A special gratitude to my supervisor Dr Poo Balan Ganesan who has guided me and continuously pushing me to do better. I extend my gratitude to family members and girlfriend who was my emotional support during the harsh time. A special thanks to my study group mates and class mates who has always guided me through all the process in the journey of my Master studies.

Table of Contents

LIST OF FIGURES

LIST OF TABLES

CHAPTER 1 INTRODUCTION

1.1 Project Background

One of the important design problems in the process industry is liquid-liquid mass transfer especially the mixing process. The stirred mixing process are energy extensive and require labor on operation and maintenance (Huibo Meng, 2016). Optimization of mixing process is an important aspect in process industries since it governs byproduct effluents and process efficiency which is important for various economic and environmental considerations (Z.Anxionnaz, 2008). The mixing efficiency affects the overall process performance since its used for wide application such as homogenization, chemical reaction, dispersion and emulsification, and heating or cooling applications (Akram Ghanem, 2014).

A static mixer has an insert-type configuration in which a series of identical, stationary inserts, called elements installed in a pipe or duct which redistribute the fluid in transverse direction to the main flow (Akram Ghanem, 2014). Static mixers redistribute the fluid by only using the kinetic energy of the flow itself (Akram Ghanem, 2014).

The static mixer gains popularity in the process industries after 1970s. However, there are older patents describe static mixer and one of them is a patent in 1874 which describes a single-element, multi-layer motionless mixer used to mix gaseous fuel with air (Sutherland, 1784). One of early french patent use helical elements in a tube to allow mixing (Petrole, 1931), and there is another paper uses multi-element design for blending solids (M.J.Bakker, 1949). Staged elements designed to promote heat transfer were patented in early 1950 (Lynn, 1958). In 2003, there are more than 2000 U.S.patents and 8000 literature articles written on motionless mixer and their application (Thakur, 2003). Despite a lot of research on motionless mixer, stirred vessel remain powerful tools in process industry especially for high viscous fluid mixing (Aubin, 2005).

"Commercial static mixers are of various types: opendesigns with helices (Helical Kenics (Chemineer, Inc.),. . .),open designs with blades or vortex generators (Low Pres-sure Drop (Ross Engineering, Inc.), Custody Transfer mixer(Komax Systems, Inc.), High-Efficiency Vortex (Chemineer,Inc.),. . .), corrugated-plates (SMV (Sulzer, Inc.),. . .), multi-layerdesigns (SMX and SMXL (Sulzer, Inc.),. . .), closed designs withchannels or holes (Interfacial Surface Generator (Ross Engi-neering, Inc.),. . .), or designs based on metallic foam inserts" (Akram Ghanem, 2014).

"Motionless inserts such as blades or corrugated plates induce changes in the fluid streamlines. Inserts with holes, channels, helical elements, and oblique blades cause local acceleration and stretching of the fluid. They split the incoming fluid into layers and then recombine the layers in a new sequence. Multilayer designs with blades and baffles split the fluid in multiple layers. These various mixing actions cause distributive mixing, by convection rather than diffusion; although to the extent that distributive mixing is high, diffusion is better able to achieve homogeneity on a molecular scale" (Akram Ghanem, 2014).

High-viscosity fluid such as in paint, cosmetic and polymer industries are usually laminar flow processes.

1.2 Problem Statement

As the innovation pushes products diversification, the multiphase mixing becomes an important aspect of process industries. The static mixer available on market satisfies the elementary conditions of mixing liquids of same phase. However, the mixing process becomes more sophisticated when multiphases mixed especially immiscible phases. Hence, a proper optimization of the static mixer configuration is needed to minimise any wastage of kinetic energy and pressure on mixing process. Proper optimization of blade twist angle and length could improve the homogeneity of mixing and reduce the pressure drop. A set blade twist angle and blade length need to be studied to find any correlation with pressure drop and mixing performance.

1.3 Project Objective

The project objectives that were identified based on the background study and the present-day problems in static mixer:

- To model static mixer with different blade configurations.

- To study the effect of blades twist angle: 180^0, 150^0, 120^0, 90^0 and length: 30mm,

    33.75mm, 37.5mm, 41.25mm and 45mm.

1.4 Project Scope

This project aims to simulate a static mixer with multiphase flow in Ansys Fluent. There are two segments for this project. The first part is validation of the simulation with a base model taken from the journal. In the validation, the pressure drop and mixing characteristics were analyzed. Then, the validated simulation used to study the effect of blade twist angle and length on pressure drop and mixing characteristics. The ansys R3 student version is used to simulate the flow. The pressure drop is characterized as pressure difference between inlet and outlet. The mixing performance characterized by observing the distribution local volume fraction of dispersed phase. Four blade twist angle were studied: 180^0, 150^0, 120^0, 90^0. Three blade length were studied: 30mm, 33.75mm, 37.5mm, 41.25mm, 45mm. All the blade twist angle studied had same length which is 37.5mm. And, all the blade length studied had same twist angle, 180^0.

CHAPTER 2 LITERATURE REVIEW

2.1 Transport Equation

Newtons second law states that the rate of change of momentum is equal to the sum of the external forces acting on the body. For a constant mass, the Newtons second law can be written in differential form as:

$$F = ma \qquad\qquad F = m\frac{dv}{dt} \qquad \text{(Equation 2.1)}$$

Where F is the forces acting on the body, v is the velocity and m is the mass of the body. When the mass of the body change with time, then equation 1 can be written as

$$F = m\frac{d(mv)}{dt} \qquad \text{(Equation 2.2)}$$

The solid body velocity is a vector quantity and can be resolved into components in the x,y,z components.

$$F_x = m\frac{d(mv_x)}{dt} \qquad F_y = m\frac{d(mv_y)}{dt} \qquad F_z = m\frac{d(mv_z)}{dt} \qquad \text{(Equation 2.3)}$$

These equations can be solved by integration to calculate the velocity at a given time if the mass and external forces acting on the body are known. In the same way, the velocity of a fluid can be calculated using Navier-Stokes equation. The Navier-Stokes equation principle is same as Newtons second law and stated as rate of change of momentum of fluid is equal to the sum of the external forces acting on a fluid (S. J. Chen, 1978). But the Navier-Stoke equation is applied to a finite volume rather than solid body and its solved using finite volume method. The Navier-Stoke equation can be written as:

$$\frac{D(mU)}{Dt} = F \qquad \text{(Equation 2.4)}$$

Where m is the mass of the finite volume, U is the velocity of the finite volume and F is the external force. Then, the equation 4 is divided by volume of fluid parcel to derive equation 5.

$$\frac{D(\rho U)}{Dt} = f \qquad \text{(Equation 2.5)}$$

Where ρ is the density of the fluid volume parcel and *f* is the sum of the external force per volume of the fluid parcel. In the same manner of Newtons second law, Navier-Stokes equation can be integrated to solve for the velocity of the fluid. When the velocity is solved, the forces acting on the solid surfaces can be determined.

In the Navier-Stokes equation, the rate of change of momentum is written in total derivative because the fluid volume may change its momentum in time and space as its moves. The total derivate can be expanded to show the change in time and change in space

$$\frac{D}{Dt} = \frac{\partial}{\partial t} + U_x \frac{\partial}{\partial x} + U_y \frac{\partial}{\partial y} + U_z \frac{\partial}{\partial z} \qquad \text{(Equation 2.6)}$$

The first term represents the change of momentum in time and the second, third and fourth term represents the change of momentum in space which is shown in x, y and z spatial directions. In vector form, the total derivative can be written in compact form as

$$\frac{D}{Dt} = \frac{\partial}{\partial t} + U . \nabla \qquad \text{(Equation 2.7)}$$

The Navier-Stokes equation can be written as in equation 8 using the expanded form of total derivative

$$\frac{\partial(\rho U)}{\partial t} + U . \nabla(\rho U) = f \qquad \text{(Equation 2.8)}$$

The interpretation of equation 8 remain same that the change of a fluid volume in time is equal to the sum of the forces acting on the fluid parcel.

The most common external forces taken into consideration when solving the fluid flow are pressure, viscosity, and gravity. These terms are included on the right-hand side of the equation

$$\frac{\partial(\rho U)}{\partial t} + \nabla.(\rho UU) = -\nabla p + \nabla.\tau + \rho g \qquad \text{(Equation 2.9)}$$

Where p is the static pressure (normal stress), τ is the shear stress and g is the acceleration due to gravitational force. The right-hand terms represent forces acting on fluid volume and the left-hand terms represents the change of momentum (velocity) due to this force. The change velocity of in response to these forces can be computed using numerical method such as finite volume method. Once the velocity computed, the forces acting on the surfaces can be computed.

In addition to solving Navier-Stokes equation to compute the velocity U, additional equation may solved depending on the application such as the convection and diffusion of quantities (velocity, temperature and concentration) in a fluid flow. All the transport equation that govern convection and diffusion share a common form (Hyun-Seob Song, 2005):

$$\frac{\partial(\rho\emptyset)}{\partial t} + \nabla.(\rho U\emptyset) = \nabla.(\Gamma\nabla\emptyset) + S_\emptyset \qquad \text{(Equation 2.10)}$$

Where $\emptyset$ is a transported quantity (concentration, temperature, and velocity etc), ρ is the density of the fluid, Γ is the diffusivity of the quantity and $S_\emptyset$ is the additional source of the quantity per unit volume.

For example, the distribution of the concentration of a fine particles or injection of dye in a fluid flow is controlled by the concentration gradient where the species moves from high concentration to low concentration. Hence the concentration C of solid particle/dye follow the equation:

17

$$\frac{\partial(\rho C)}{\partial t} + \nabla.(\rho U C) = \nabla.(D\nabla C) + S_c \qquad \text{(Equation 2.11)}$$

Where D is the diffusivity of the particles, S_c is the source term of the particles transported. This equation is called a transport equation because the concentration C of the particles is transported by the velocity of fluid.

The concentration of the particles is transported through the fluid by two mechanism: convection and diffusion. Diffusion is a physical process where the particles moves from the areas of higher concentration to lower concentration. The diffusion of the particles can be represented by mathematical form:

$$\nabla.(D\nabla C) = \frac{\partial}{\partial x}\left(D\frac{\partial C}{\partial x}\right) + \frac{\partial}{\partial y}\left(D\frac{\partial C}{\partial y}\right) + \frac{\partial}{\partial z}\left(D\frac{\partial C}{\partial z}\right) \qquad \text{(Equation 2.12)}$$

The diffusivity D gives the strength of diffusion. A high diffusivity will transfer significant quantity of particles with a small concentration gradient. On the other hand, a low diffusivity will transfer small quantity of particles even with high concentration gradient. Diffusion occurs in a moving or a stationary fluid hence its independent of fluid velocity U.

Convection is the transport of the particles by motion of the fluid U. This represented by mathematical form:

$$\nabla.(\rho U C) = \frac{\partial}{\partial x}(\rho C U_x) + \frac{\partial}{\partial y}\left(\rho C U_y\right) + \frac{\partial}{\partial z}(\rho C U_z) \qquad \text{(Equation 2.13)}$$

The particles physically transported by the motion of the fluid U. This is like the transport of the boats in a river which are carried away by the flow of the river. The velocity of the river U pushes the boat along the flow.

2.2 Multiphase Flow

Mixture Model

The mixture model uses a single-fluid approach. In the mixture model, the different phases allowed to interpenetrate. The volume fraction for a phase in a control volume can vary between 0 and 1 depending on the space occupied by the particular phase. The slip velocity concept in mixture model allows the phases to move at different velocity.

The equation solved in mixture model are:

- Continuity equation for the mixture

- Momentum equation for the mixture

- Energy equation for the mixture (If heat transfer involved)

- Volume fraction equation for the secondary phase

- Algebraic expressions for the relative velocities (if phases move at different velocity)

Continuity Equation

The mixture model continuity equation is

$$\frac{\partial}{\partial t}(\rho_m) + \nabla.(\rho_m \overrightarrow{v_m}) = \dot{m} \qquad \text{(Equation 2.14)}$$

Where $\overrightarrow{v_m}$ is the mass-averaged velocity:

$$\overrightarrow{v_m} = \frac{\sum_{k=1}^{n} \alpha_k \rho_k \overrightarrow{v_k}}{\rho_m} \qquad \text{(Equation 2.15)}$$

and ρ_m is the mixture density:

$$\rho_m = \sum_{k=1}^{n} \alpha_k \rho_k \qquad \text{(Equation 2.16)}$$

α_k is the volume fraction of phase k, $\dot{m}$ is the mass transfer due to cavitation.

Momentum Equation

The momentum equation is obtained by summing up all the momentum equation of the phases (M.M. Haddadi, 2020). The mathematical expression:

$$\frac{\partial}{\partial t}(\rho_m \overrightarrow{v_m}) + \nabla.(\rho_m \overrightarrow{v_m}\overrightarrow{v_m}) = -\nabla p + \nabla.[\mu_m(\nabla \overrightarrow{v_m} + \nabla \vec{v}_m^T)] \rho_m \vec{g} + \vec{F} +$$

$$\nabla.(\sum_{k=1}^{n} \alpha_k \rho_k \vec{v}_{dr,k} \vec{v}_{dr,k}) \qquad \text{(Equation 2.17)}$$

Where n is the number of phases, $\vec{F}$ is a body force, μ_m is the viscosity of the mixture:

$$\mu_m = \sum_{k=1}^{n} \alpha_k \mu_k \qquad \text{(Equation 2.18)}$$

$\vec{v}_{dr,k}$ is the drift velocity for secondary phase k:

$$\vec{v}_{dr,k} = \vec{v}_k - \vec{v}_m$$

Energy Equation

Energy equation for mixture:

$$\frac{\partial}{\partial t}\sum_{k=1}^{n}(\alpha_k \rho_k E_k) + \nabla.\sum_{k=1}^{n}(\alpha_k \vec{v}_k (\rho_k E_k + p)) = \nabla.(k_{eff}\nabla T) + S_E \quad \text{(Equation 2.19)}$$

Where k_{eff} is the effective conductivity (k+k_t, where k_t is the turbulent thermal conductivity, defined according to the turbulence model being used). The first term on the right-hand side of equation 19 represents energy transfer due to conduction. S_E is any other heat source.

$$E_k = h_k - \frac{p}{\rho_k} + \frac{v_k^2}{2} \qquad \text{(Equation 2.20)}$$

for a compressible phase, and $E_k = h_k$ for an incompressible phase, where h_k is the sensible enthalpy for phase k.

<u>Volume Fraction Equation</u>

From the continuity equation for secondary phase p, the volume fraction equation for secondary phase p can be obtained:

$$\frac{\partial}{\partial t}\left(\alpha_p \rho_p\right) + \nabla.\left(\alpha_p \rho_p \vec{v}_m\right) = -\nabla.\left(\alpha_p \rho_p \vec{v}_{dr,p}\right) \qquad \text{(Equation 2.21)}$$

<u>Relative (Slip) Velocity and Drift Velocity</u>

The slip velocity is the velocity of secondary phase (p) relative to the primary phase (q):

$$\vec{v}_{qp} = \vec{v}_p - \vec{v}_q \qquad \text{(Equation 2.22)}$$

The drift velocity and the relative velocity ($\vec{v}_{qp}$) are connected by the following expression:

$$\vec{v}_{dr,p} = \vec{v}_{qp} - \sum_{k=1}^{n}\frac{\alpha_k \rho_k}{\rho_m}\vec{v}_{qk} \qquad \text{(Equation 2.23)}$$

The mixture model uses algebraic slip formulation. The algebraic slip mixture model prescribes an algebraic relation for relative velocity, a local equilibrium should be reached over short spatial length scales (Vimal Kumar, 2008). The mathematical form of the relative velocity is:

$$\vec{v}_{qp} = \tau_{qp}\vec{a} \qquad \text{(Equation 2.24)}$$

Where $\vec{a}$ is the secondary-phase particles acceleration and τ_{qp} is the particulate relaxation time. τ_{qp} is of the form (Manninen):

$$\tau_{qp} = \frac{(\rho_m - \rho_p)d_p^2}{18\mu_q f_{drag}} \qquad \text{(Equation 2.25)}$$

Where d_p is the diameter of the particles of the secondary phase p, and the drag function f_{drag} is from Schiller and Naumann:

$$f_{drag} = \begin{cases} 1 + 0.15Re^{0.687} & Re \leq 1000 \\ 0.0183Re & Re > 1000 \end{cases} \qquad \text{(Equation 2.26)}$$

and the $\vec{a}$ could be expressed as

$$\vec{a} = \vec{g} - (\overrightarrow{v_m}.\nabla)\overrightarrow{v_m} - \frac{\alpha\overrightarrow{v_m}}{\partial t} \qquad \text{(Equation 2.27)}$$

The drift flux model is the simplest algebraic slip formulation in which the acceleration of particles given by gravity and centrifugal force and the particulate relaxation time takes account the other particles presence.

The mixture would be reduced to homogeneous multiphase model if the slip velocity is not solved.

2.3 Finite Volume Method

Finite volume method is a method of converting the partial differential equation into algebraic form expression and solving it (Pedro F. Lisboa, 2010). In this method, the divergence theorem used to convert volume integral that contain divergence term into surface integral. These terms are evaluated as the fluxes at surfaces and balanced within a control volume. The fluxes entering a volume should be equal to fluxes exiting a control volume and for this reason it's a conservative method.
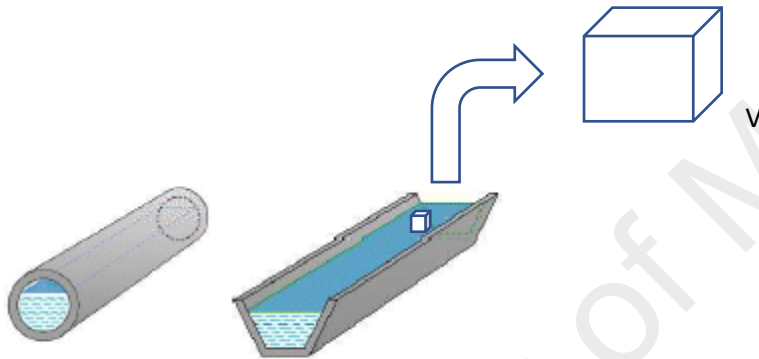

Figure 2.1 A finite volume of fluid from a fluid flow channel

Divergence theorem

According to divergence theorem, the rate of accumulation of a vector field inside a control volume is equal to the flux of the vector field across the surfaces of control volume.

$$\int_v (\nabla . A)dV$$

Flux out

$$\int_A (A.\hat{n})dA$$

Accumulation of matter in the volume
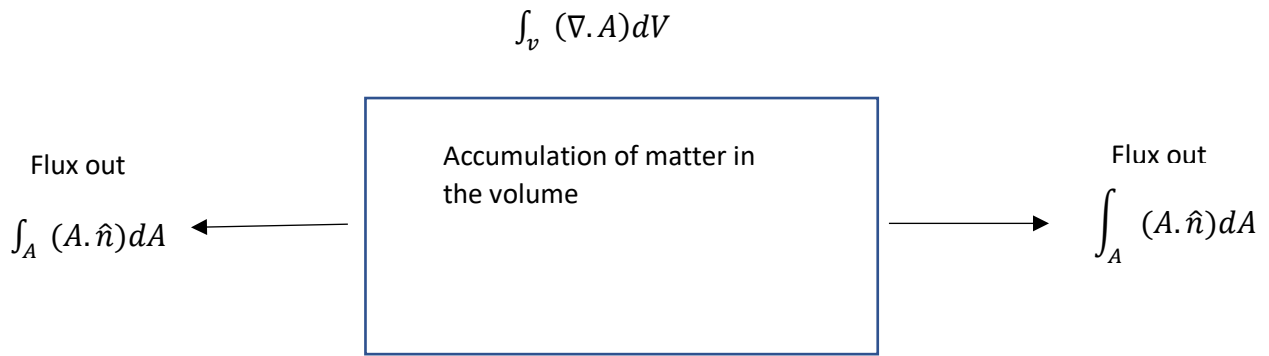
Flux out

$$\int_A (A.\hat{n})dA$$

Figure 2.2 This diagram depicts the divergence theorem. The accumulation of particles within the volume is equal to the fluxes around the surface.

In the mathematical form, the divergence theorem is written as

$$\int_v (\nabla . A)dV = \int_A (A.\hat{n})dA \qquad \text{(Equation 2.28)}$$

$$\int_v \left(\frac{\partial A_x}{\partial x} + \frac{\partial A_y}{\partial y} + \frac{\partial A_z}{\partial z}\right)dV = \int_A (A_x n_x + A_y n_y + A_z n_z)dA \qquad \text{(Equation 2.29)}$$

A is the surface area of the control volume.

Interior Cells and Boundary Cells

Any body or flow region will be divided into fine mesh (finite volume) to solve the problem numerically. When dividing the body into finite volume, there will be two types of cells: the interior cell and the boundary cell. The interior cells are the cell which wholly surrounded by other cells, it shares all the faces with other neighbouring cells. The boundary cells are the cell which share one or more faces with boundary condition which would be defined by the problem.

1)Interior cell   2) Boundary cell

Figure 2.3 The interior cell and the boundary cell

Central-differencing method

Interior Cells

For example, lets take concentration gradient (in diffusion term) to illustrate how the interior cell equation is derived.

$$\frac{dC}{dx} = \frac{\Delta C}{\Delta x} = \frac{Change\ in\ Concentration}{Distance}$$

Let's take letter l and r to denote the concentration gradient on the left surface and right surface. To solve this temperature gradient on the surfaces, the temperature at the cell centroids (L,R and P). This can be solved by linear interpolation, which is called as central-differencing.
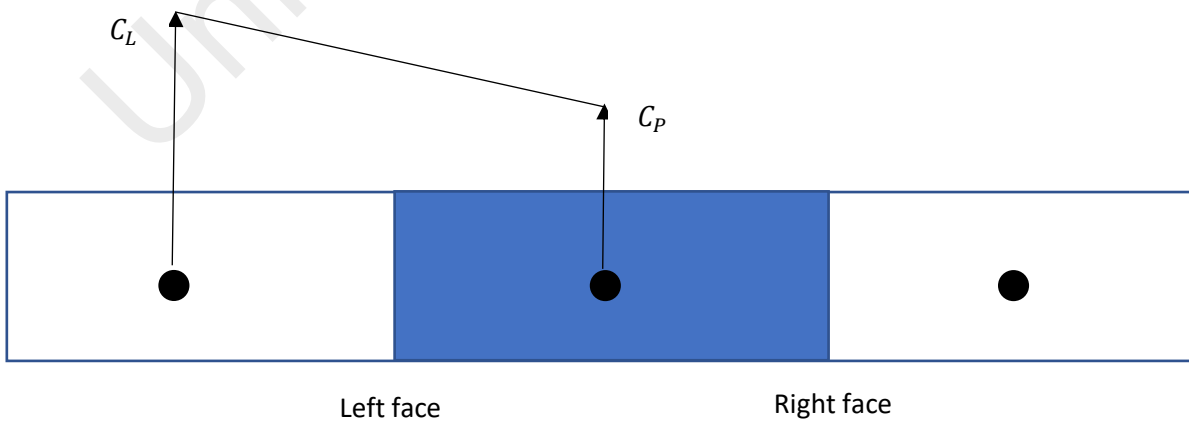

Figure 2.4 The illustration of central differencing on the left face

As shown in figure 2.4, the concentration gradient on the left face can be expressed using central differencing as:

$$\left(\frac{dC}{dx}\right)_l = \frac{C_P - C_L}{d_{LP}}$$

Where d_{LP} is the distance between cell centroids L and P. In same way, the concentration gradient on the right face can be expressed using the central differencing:

$$\left(\frac{dC}{dx}\right)_r = \frac{C_R - C_P}{d_{PR}}$$

This method also can be extended to convection term in which we need to find the concentration on the left face C_l and the right face C_r rather than concentration gradient. For this, we will take the average of centroid temperature of neighbour cells.

$$C_l = \frac{1}{2}(C_L + C_P)$$

and for the right face:

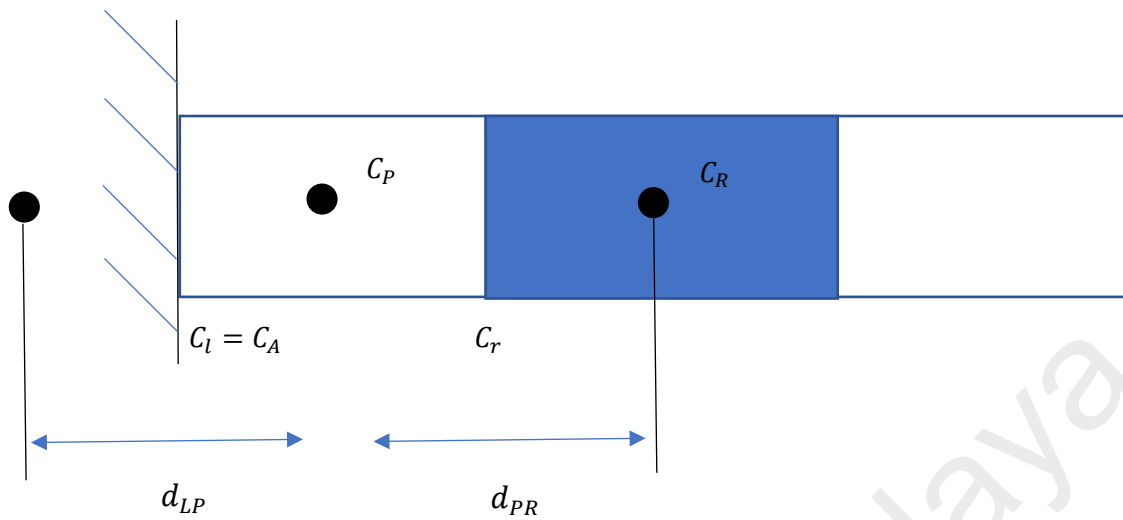$$C_r = \frac{1}{2}(C_P + C_R)$$

Boundary Cell (left)

Figure 2.5 The left boundary cell with centroid temperature of C_p and shares the face with right cell at C_r and boundary cell at $C_l = C_A$.

The concentration gradient on the left face can be expressed as:

$$\left(\frac{dC}{dx}\right)_l = \frac{C_P - C_A}{d_{LP}/2}$$

The concentration gradient on the right face follows the derivation as shown in the interior cells' derivation part.

For the convection term, we need to find the concentration on the face rather than concentration gradient. For this, the left face concentration will be:

$$C_l = C_A$$

and the right face concentration will be:

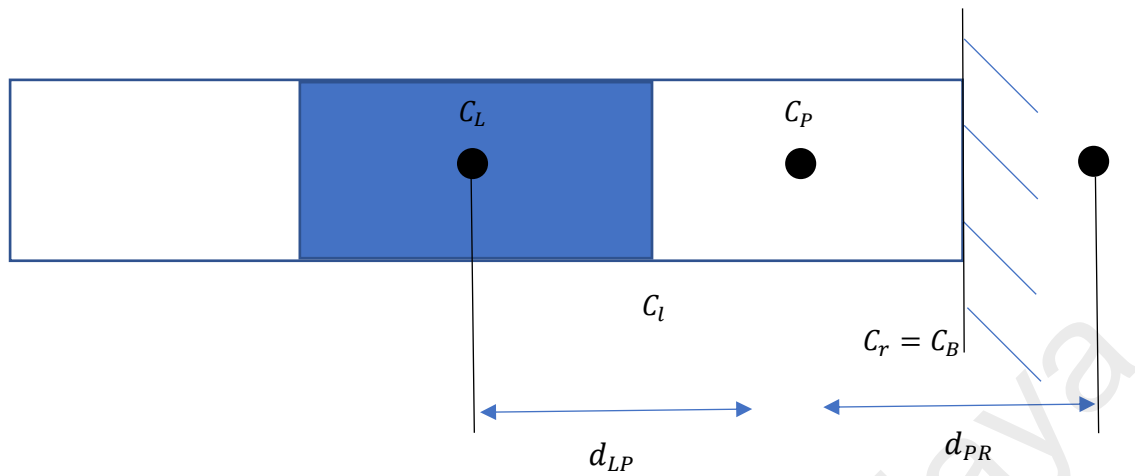$$C_r = \frac{1}{2}(C_P + C_R)$$

Boundary Cell (right)

Figure 2.6 The right boundary cell with centroid temperature of C_p and shares the face with left cell at C_l and boundary cell at $C_r = C_B$.

The concentration gradient on the right face can be expressed as:

$$\left(\frac{dC}{dx}\right)_r = \frac{C_B - C_P}{d_{PR}/2}$$

The concentration gradient on the left face follows the derivation as shown in the interior cells' derivation part.

And for the convection term, the right face concentration will be:

$$C_r = C_B$$

and the left face concentration is:

$$C_l = \frac{1}{2}(C_L + C_P)$$

<u>Upwind-differencing method</u>

When the Peclet number is >2, non-physical oscillations are generated in the solution. An alternative to the central differencing scheme which does not lead to non-physical oscillation is an upwind scheme. The upwind differencing scheme is applied to the convection term where derivation of the face concentration needed. In the upwind scheme, the concentration on the face takes value of upwind cell centroid which means the value at the cell centroid in the direction of flow.
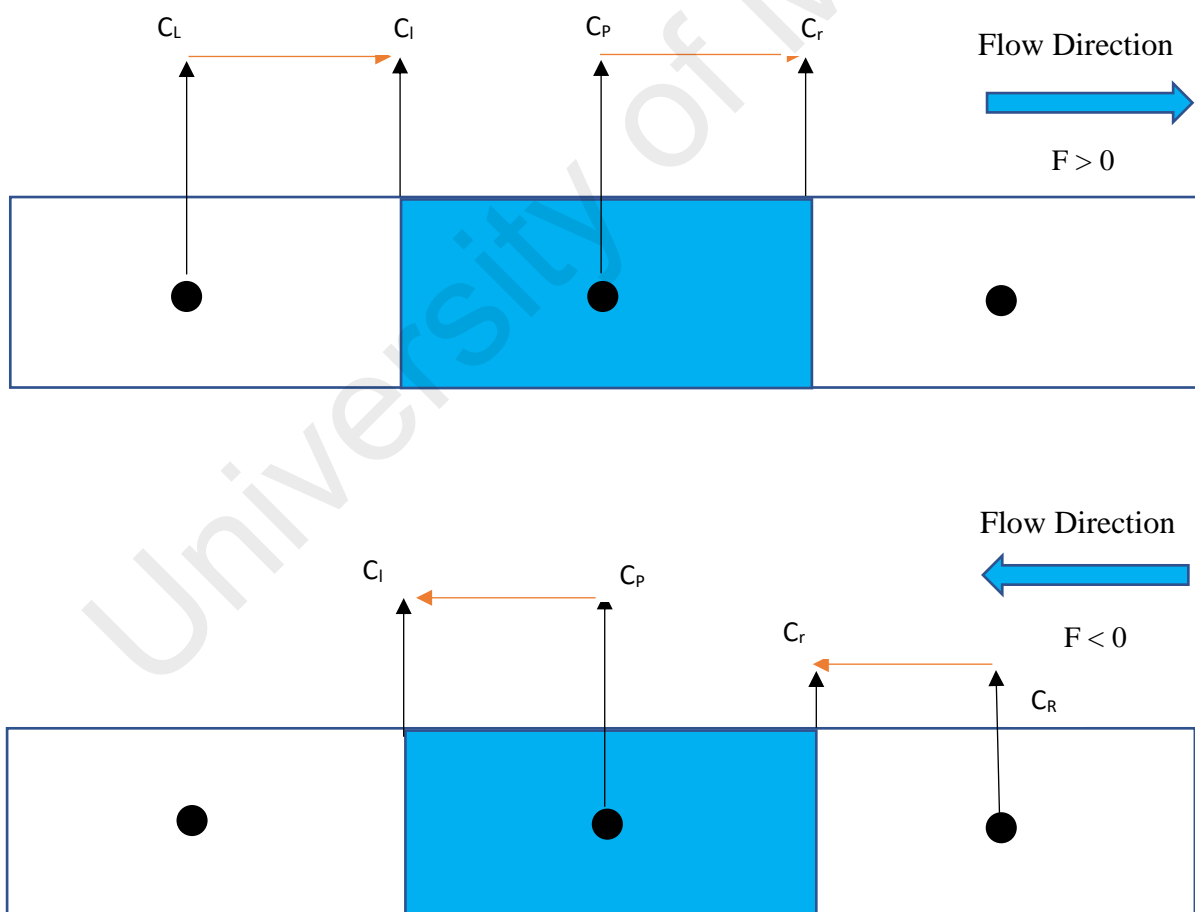
Interior cells

Figure 2.7 This figure illustrate how the concentration of the left face and the right face of the cell computed when the flow is right to left F>0 and the flow is left to right F<0

These two cases can precisely written as:

$$C_l = \begin{cases} C_L & F > 0 \\ C_P & F < 0 \end{cases}$$

and

$$C_r = \begin{cases} C_P & F > 0 \\ C_R & F < 0 \end{cases}$$

Boundary Cell (left)

In the same way as the interior cell is illustrated, two different flow direction will be derived for the left boundary cell.

$$C_l = \begin{cases} C_A & F > 0 \\ C_P & F < 0 \end{cases}$$

and

$$C_r = \begin{cases} C_P & F > 0 \\ C_R & F < 0 \end{cases}$$

Boundary Cell (right)

In the same way the left boundary cell face concentration illustrated, the right boundary cell face concentration could be expressed:

$$C_l = \begin{cases} C_L & F > 0 \\ C_P & F < 0 \end{cases}$$

and

$$C_r = \begin{cases} C_P & F > 0 \\ C_B & F < 0 \end{cases}$$

CHAPTER 3 METHODOLOGY

3.1 Validation of Simulation

A case study is taken from the paper (Z.Jaworski, 2002) to validate the simulation. Then, the simulation is modified to serve the objective of this paper.

The Base Model

The base model for validation is taken from the journal (Z.Jaworski, 2002). This model contains 10 standard Kenics inserts. The twisted Kenics mixer blades were placed alternatively in clockwise and anti-clockwise. A single Kenic Mixer dimension is 25mm for the diameter, 37.5mm for the height and 3mm for the thickness. The inlet tube length is 90mm and the exit tube length is 70m. There is a internal tube with a diameter of 1 mm is placed at entrance which is used to introduce the dispersed phase into the tube. The first insert of the Kenics mixer is clockwise twisted similar to the paper.
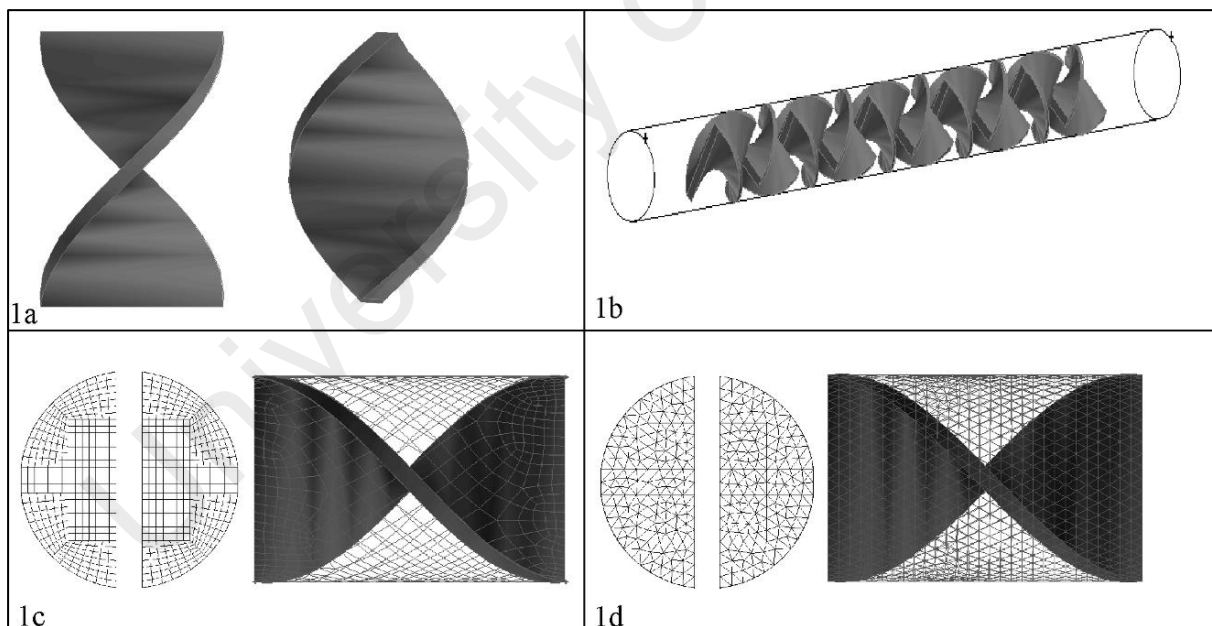

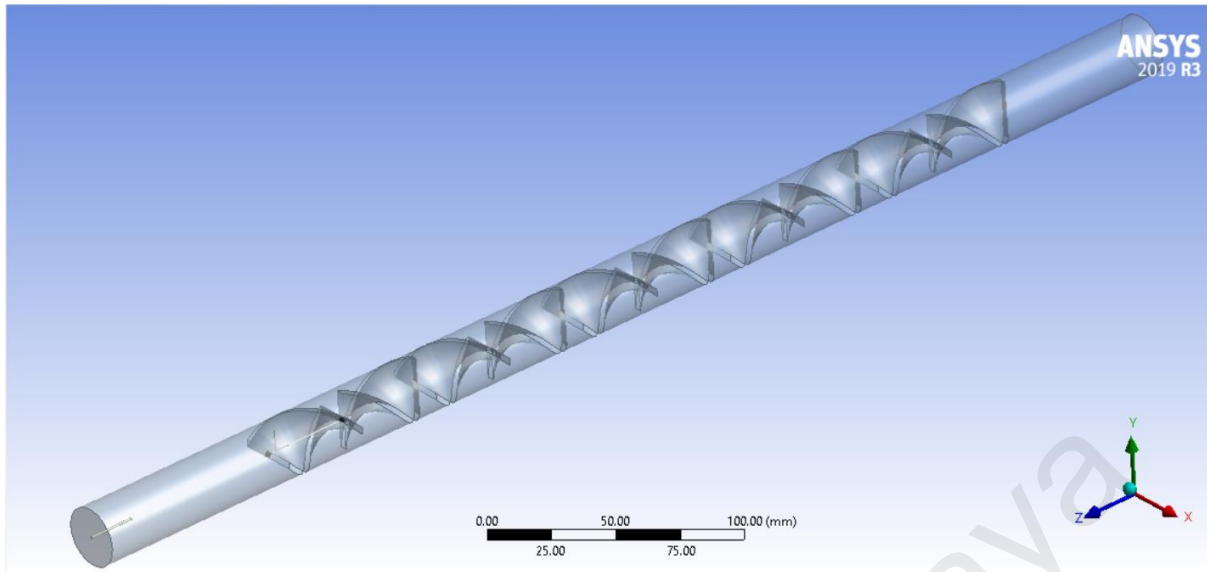Figure 3.1 The Kenics Model used for the validation. (Z.Jaworski, 2002)

Figure 3.2 The model created based on the dimension given in the paper (Z.Jaworski, 2002)

The blade is 180 degree twisted and arranged clockwise and anti-clockwise. First a rectangular blade is formed, then it twisted using sweep function (FD5, turns = 0.5). Then, ten patterns are created with FD1 offset of 37.5mm. Then, five alternate blades were chosen rotation (90-degree rotation). After that, the 10 mixer blades united using Boolean function. Then, two cylinders are created. One is the outer body of the Kenics mixer and another one is the small internal tube for dispersed phase delivery. The outer tube length is 535mm and the internal tube length is 20mm. Finally, the Boolean tool is used to substract the kenics blade from the long tube.

Meshing

The second part of simulation is meshing. The structured meshing method is used to generate a coarse meshing for the simulation. The tools used for meshing is body meshing, face meshing, edge meshing and tetrahedron method to generate the desired mesh. However, the (Z.Jaworski, 2002) paper uses hexahedral mesh for the structured meshing. It was not possible to replicate the exact meshing method due to convergence instability issue. Hence, tetrahedron is adopted instead of hexahedral. The tetrahedron is more stable for highly complex geometry with sharp bents. The mesh created were shown on figure 3.3.
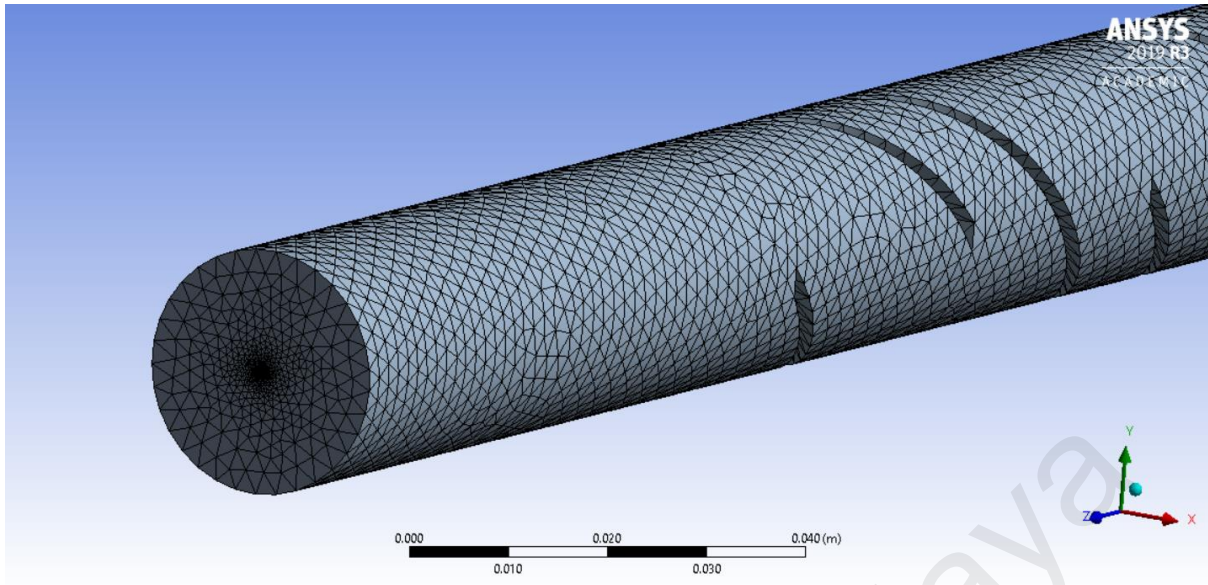
Figure 3.3 The mesh created for the simulation

The various method used for the mesh generation were summarized in table 3.1

Table 3.1 The method and sizing used for mesh generation

Component	Method	Element Size (m)
Internal tube	Body Sizing	0.00015
	Edge Sizing	0.00015
	Tetrahedron	-
External tube	Body Sizing	0.0025
	Edge Sizing	0.0025
	Face Sizing	0.0025
	Tetrahedron	-
Mixer Blade	Face Sizing	0.0025

and after that several faces were named as inlet_dispersed, inlet_continuous, outlet_end, wall_dispersed, mixer wall, continuous_flow_domain and dispersed_flow_domain for setting up boundary condition later on in model.
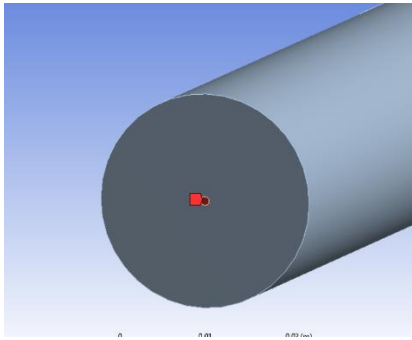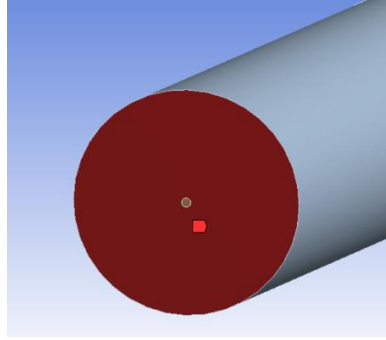
a)   b)

Figure 3.4 a) the dispersed phase inlet and b) the continuous phase inlet

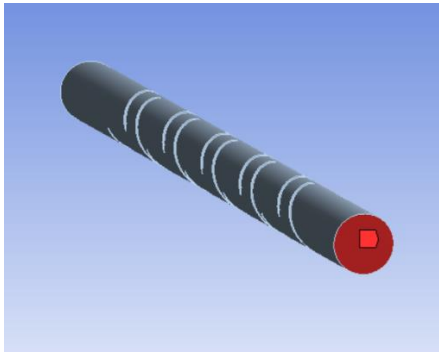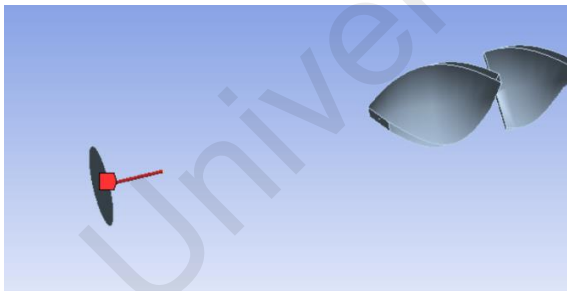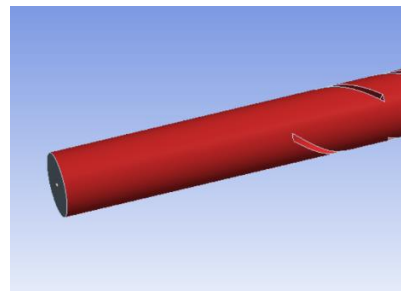Figure 3.5 The outlet end

a)   b)

Figure 3.6 a)The dispersed phase tube wall and b) the mixer wall

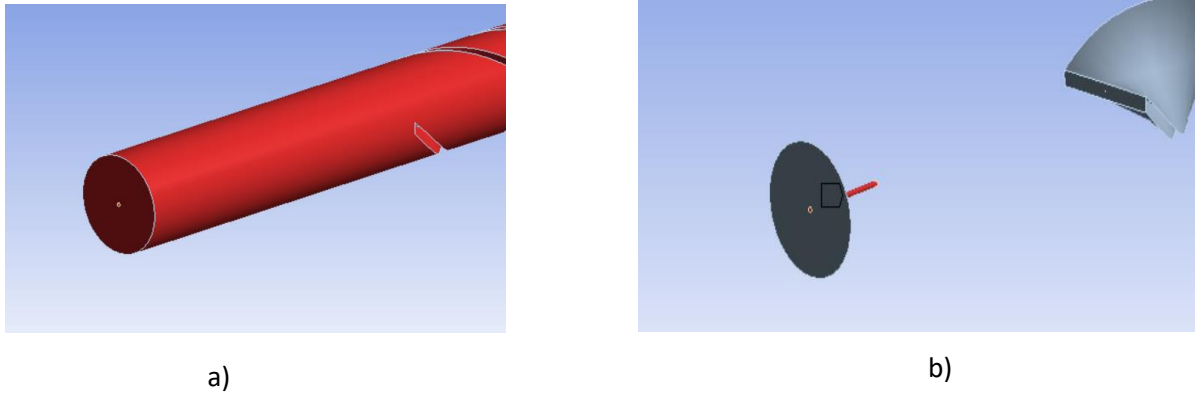a)   b)

Figure 3.7 a) The continuous flow domain and b) the dispersed flow domain

Boundary Set up

The modelling was carried out for two cases of two-phase laminar flow. In both the cases, the continuous phase is an aqueous solution of refined CMC with a dynamic viscosity of 0.050 Pa.s and the dispersed phase is the silicon oil 50 (dynamic viscosity 0.047 Pa.s and silicon oil 500 (dynamic viscosity 0.479 Pa.s). The liquid density of refined CMC is 998 kg/m^3, silicon oil 50 is 949 kg/m^3 and silicon oil 500 is 957 kg/m^3. Surface tension in refined CMC is 0.0249 N/m and 0.0243 N/m for silicon oil 50 and silicon oil 500. The velocity at inlet was set according to table 3.2.

Table 3.2 The continuous (CMC) and dispersed (silicon oil) phase velocities, oil drop size, and Weber number for different Reynolds number (Z.Jaworski, 2002)

Reynold number, Re	Mean inlet velocity, m/s		Oil drop diameter, $d_{32, \mu m}$		Weber number, We	
	Continuous phase, v_q	Dispersed phase, v_p	Oil 50	Oil 500	Oil 50	Oil 500
100	0.202	1.28	1753	2610	40.6	41.6
200	0.405	2.56	620	923	163	167
400	0.811	5.11	219	326	650	666

The Numerical Model

The mixture model with algebraic slip mixture (ASM) is used in this simulation. The model allows mutual interpenetration of the phases. " In steady-state simulations with ASM model, a standard set of continuity and momentum (Navier-Stokes) equations is solved for the whole two-phase mixture, treated as continuum, and additionally the continuity equation for the dispersed phase (p) is included" (Z.Jaworski, 2002).

"The model offers computations of the local volume fraction and velocity of two flowing phases". The drop size of the dispersed phase assumed to be constant.
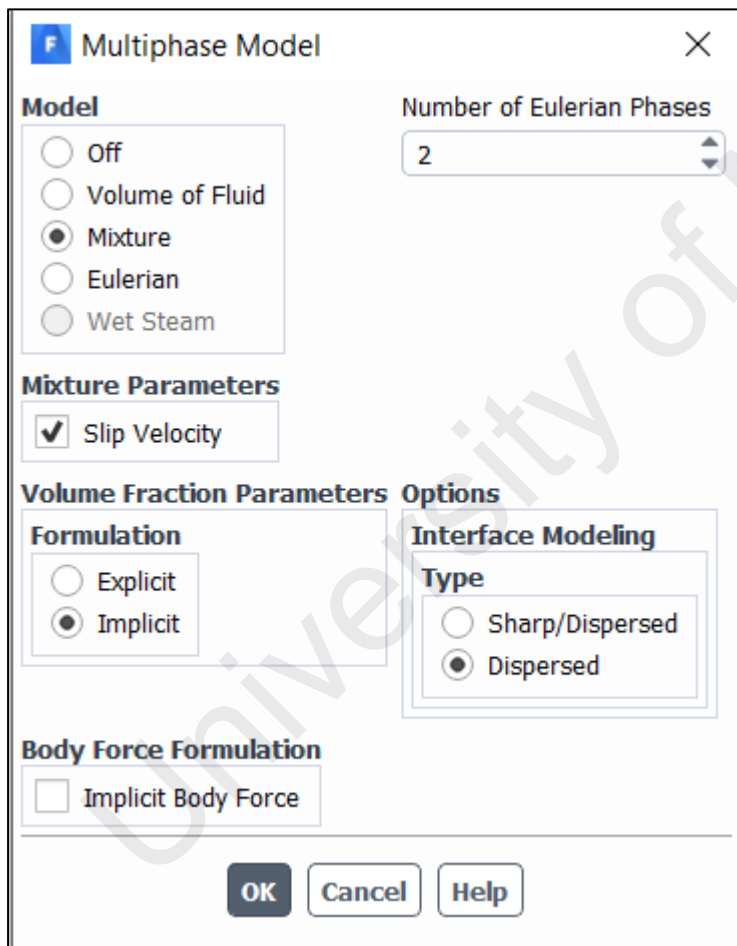

Figure 3.8 The model used for the simulation

The mixture model is used with the slip velocity is turned on. The volume fraction formulation is set to implicit and interface modelling is dispersed.

The continuous phase is set with refined CMC solution and the dispersed phase is set with silicon oil 50 and silicon oil 500.
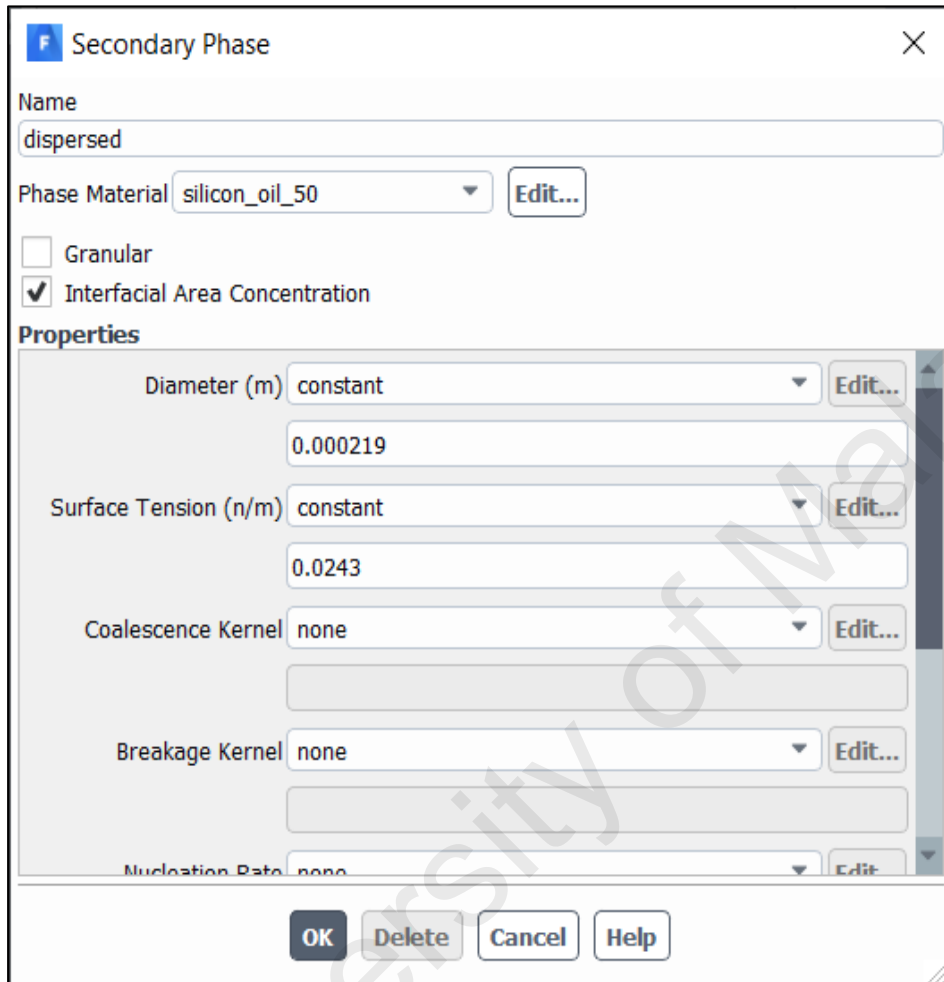

Figure 3.9 The secondary phase

The interfacial area concentration function is used for secondary phase with a constant diameter as per from table 3.2

Then, the continuous phase velocity and dispersed phase velocity is set as per table 3.2. The volume fraction of the oil for the continuous phase is set to zero and unity for dispersed phase. The computation is carried out with standard set of underrelaxation factors. The wall condition is set to no slip condition. The outlet is set to pressure outlet. The standard pressure-velocity coupling solver is used.
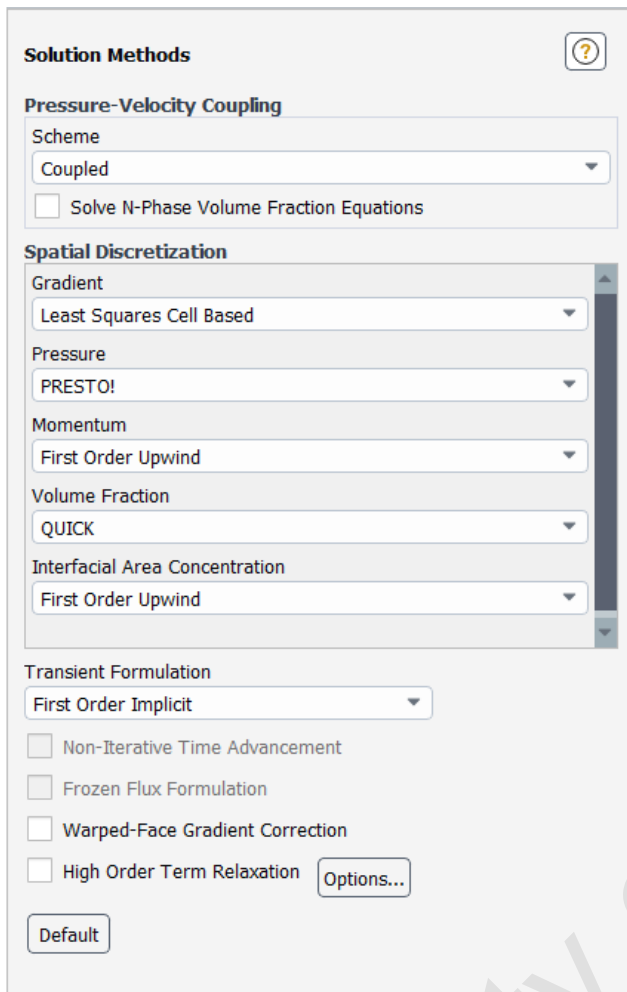
Figure 3.10 The solution method used in the simulation

After completing the simulation the pressure drop across one mixer blade is compared with the paper (Z.Jaworski, 2002) to validate. The mixing efficiency of the two liquids is evaluated using the local volume fraction distribution for the dispersed phase (Z.Jaworski, 2002).

3.2 The blade twist angle and lenghth modification

After completing the validation, one of the case study is used to further investigate the effect of blade twist angle and the length on the pressure drop and mixing efficiency. The case selected was silicon oil 50 with Reynolds 400. The geometrical modification carried out is represented on the table 3.3

Table 3.3 The geometrical setting for various blade twist angle

Blade Twist Angle	FD5, Turns	Blade Rotation
180^0	0.5	90^0
150^0	0.417	120^0
120^0	0.333	150^0
90^0	0.25	180^0

The FD5 represnts the turns setting under sweep function to get desired blade twist angle. The blade rotation is the appropriate rotation of the blade to get a 90 degree rotation.
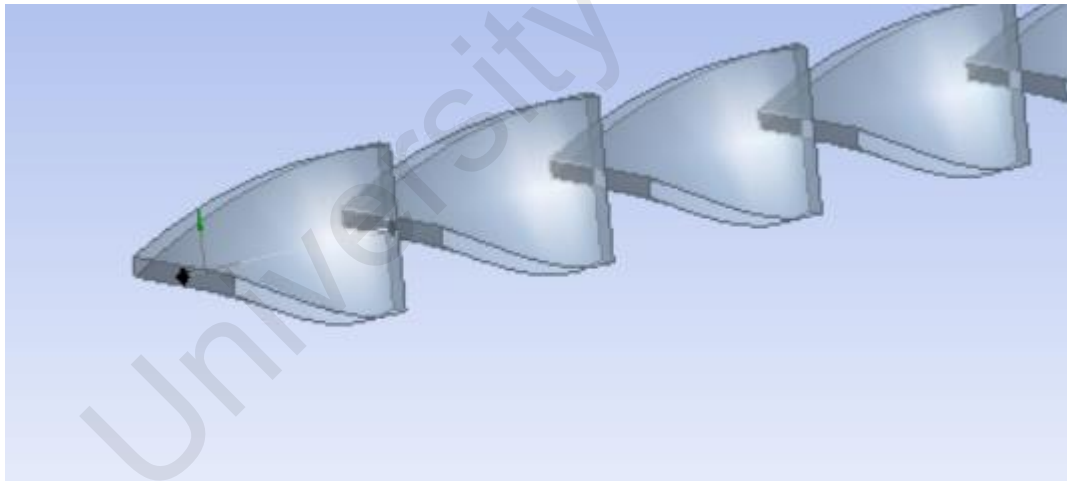

Figure 3.11 A 90 degree twist blade.

For a 90 degree twist, the blade rotation is set to 180 degree so that each blade exit is 90 degree to another blade entrance.

3.3 The Pressure Drop Calculation

Two planes are created to calculate the pressure drop: 1) 0.01m before the first insert (Inlet pressure, P1) and 2) 0.01m after the last insert (Outlet pressure, P2). Then, the area-averaged pressure at the inlet and outlet is taken from ansys post-processing. The difference between these pressure (P1 – P2) is treated as pressure drop across the mixer blades.
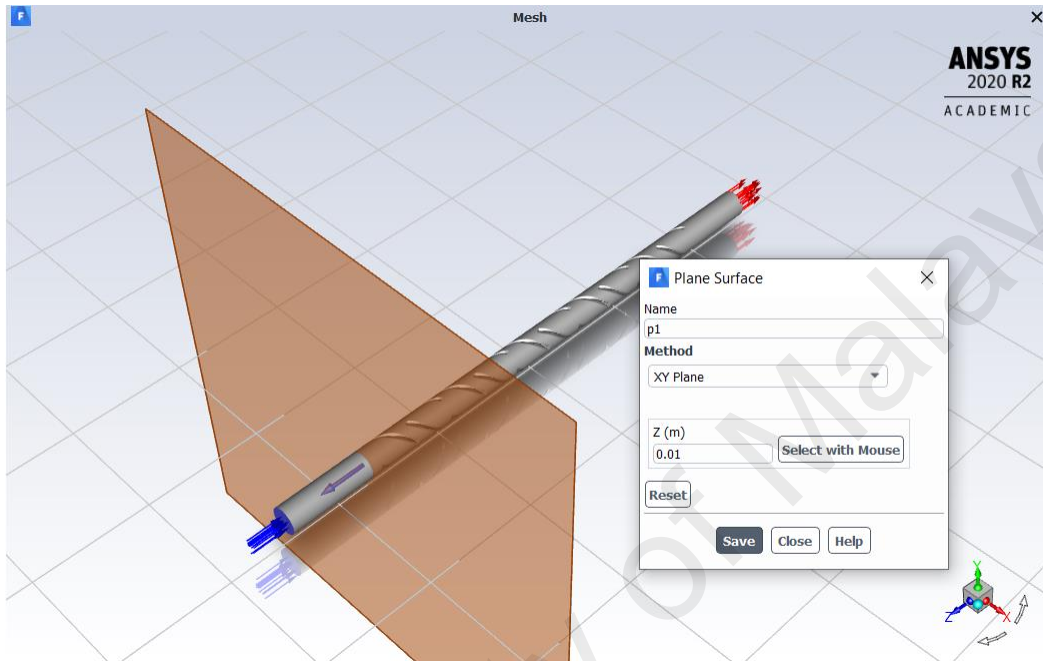

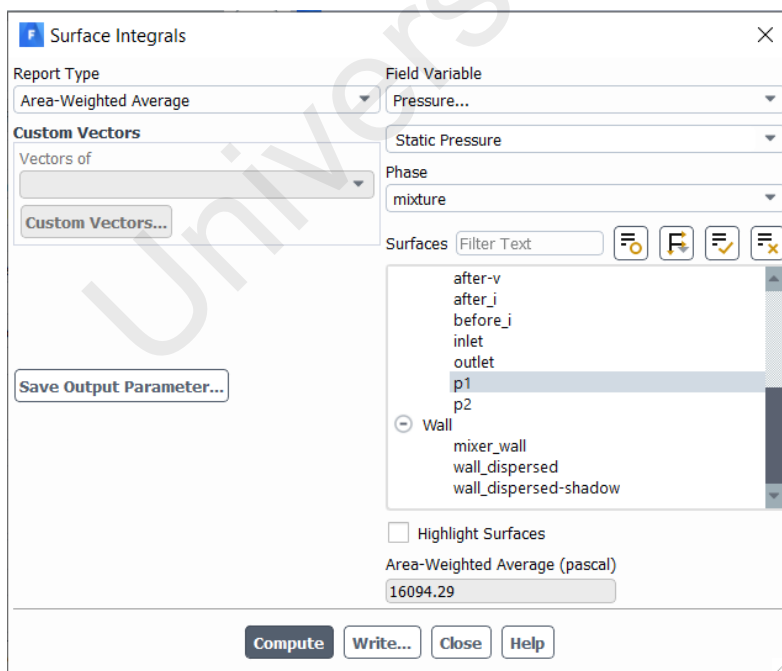Figure 3.12 The Plane created for inlet pressure, P1

Figure 3.13 Surface integral to compute area averaged pressure

3.4 Quantitative Analysis of Mixing Performance

The quantitative analysis of mixing performance is conducted by analysis the uniformity index of dispersive phase volume fraction across several planes. The planes where created according to table 3.4. Then, the area averaged uniformity index at each blade is commuted as shown in figure 3.12.

Table 3.4 The planes created across the static mixer blade to compute mixing performance

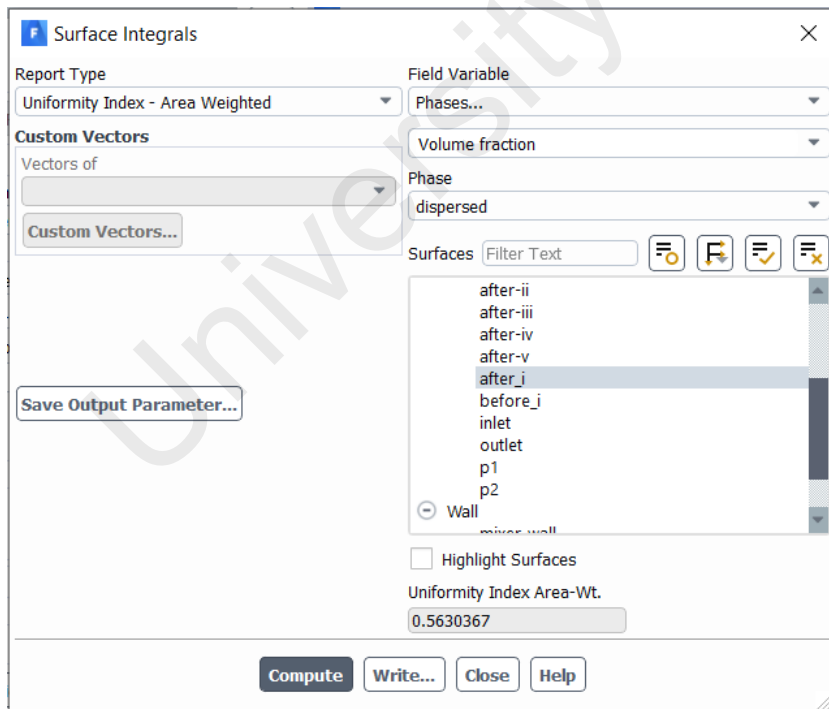| Planes	Position on Z axis, m
Inlet	0
Before I Insert	0.07
After I Insert	0.1075
After II Insert	0.145
After III Insert	0.1825
After IV Insert	0.22
After V Insert	0.2575
Outlet	0.515

Figure 3.14 Surface Integral to compute area weighted uniformity index

3.5 Qualitative Analysis of Mixing Performance

The qualitative analysis of mixing performance is carried out by evaluating the dispersed phase volume fraction contour across the mixer blade. The planes were created according to the position based on table 3.4. Then, the contour of dispersed phase volume fraction is created for each planes. After that, the contours were compared and studied. A constant range of 0 to 0.00975 local dispersed phase volume fraction is used for all the studies.
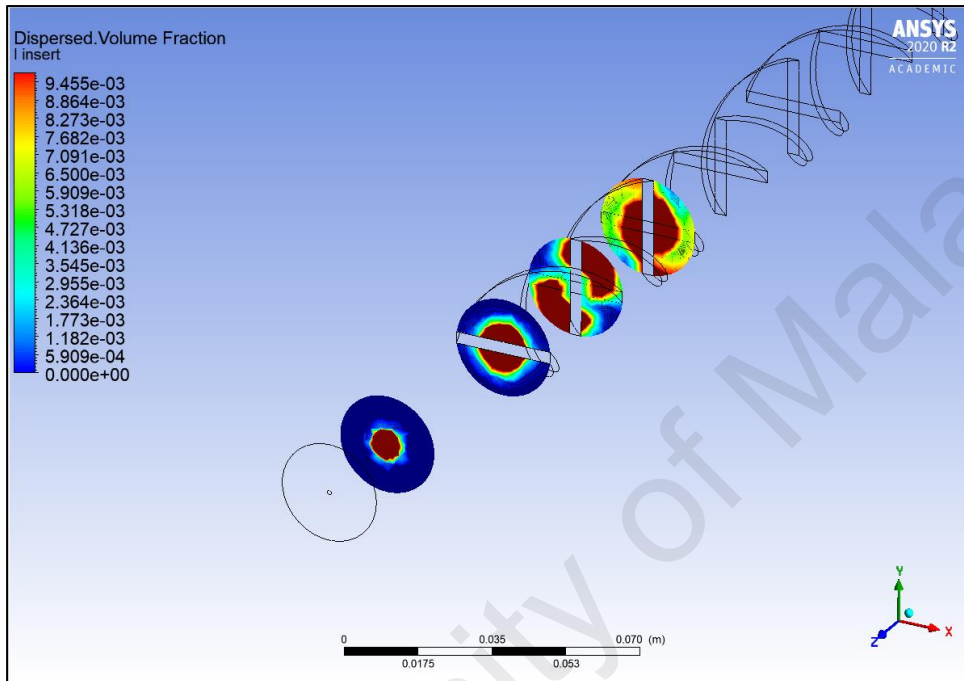

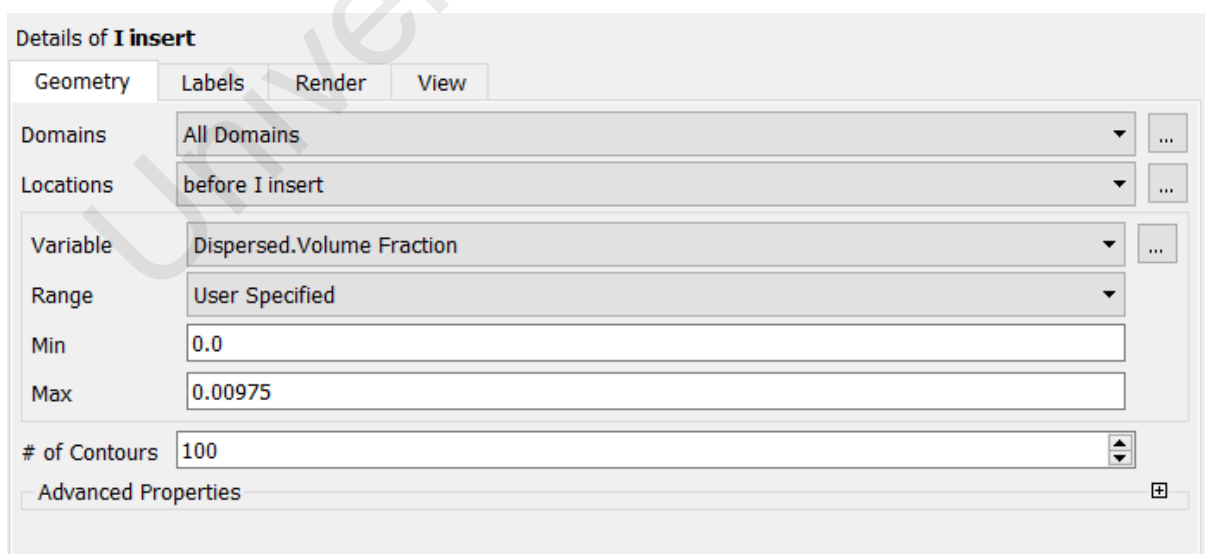Figure 3.15 The planes created across the mixer blades.

Figure 3.16 The Range of dispersed phase volume fraction used
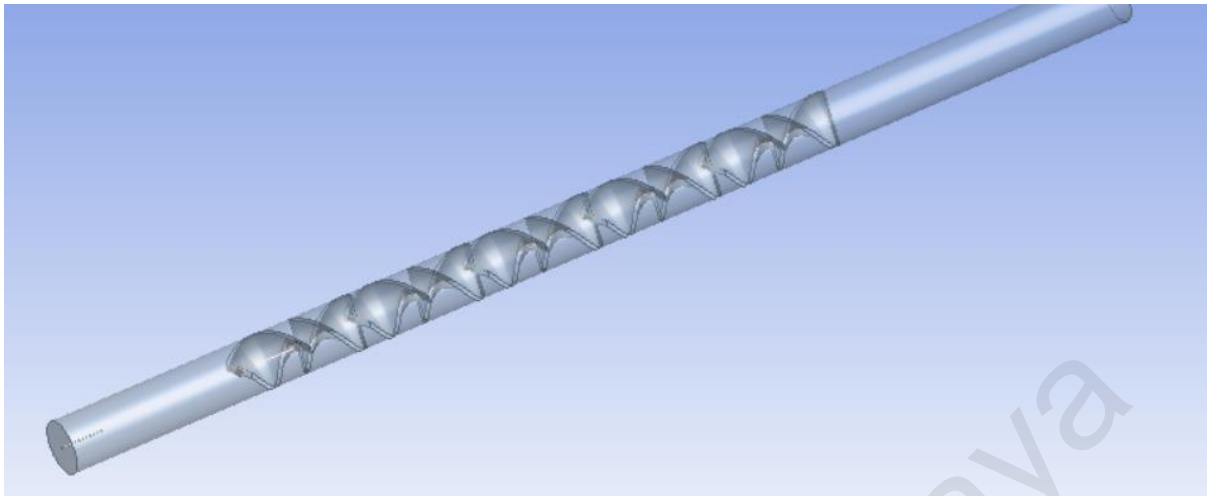
Length Modification

Figure 3.12 Static mixer with shorter blade length (30mm)

The blade with 180 degree twist angle is chosen to further investigate the effect of mixer blade length on the pressure drop and mixing efficiency. The length variation used was 30mm, 37.5mm and 45mm. This is to study how decreasing and increasing blade length affects the mixing process.

CHAPTER 4 RESULTS AND DISCUSSION

4.1 Validation of Simulation

The table 4.1 shows the pressure drop for Silicon Oil 50 and Silicon Oil 500 under three different flow condition (Reynolds number of 100, 200 and 400). The P1 is the area-weighted average of pressure at the starting point of the mixer blade and P2 is the area-weighted average of pressure at the end of the mixer blade. Then, the difference between these values computed as pressure drop. $\Delta P *$ is the estimates from the reference "Figure 2. Pressure drop in the Kenics static mixer vs Reynolds number, refined CMC solution. Silicon oil 50, block-structured grids (2a), unstructured grids (2b) and refined CMC solution – silicon oil 500, block structured grid (2c)" (Z.Jaworski, 2002).

Both the silicon oil 50 and silicon oil 500 shows a good agreement with the journal for the Reynolds number of 100 and 200. The pressure drop for Reynold number 100 of silicon oil 50 averages at 2 to 3 kPa and pressure drop for Reynold number 200 of silicon oil 500 averages at 5 to 6kPa. For silicon oil 500, the pressure drop for Reynold number 100 averages at 2 to 3 kPa and Reynold number 200 averages at 6kPa. However, there is a large difference of pressure drop between simulation and journal when it comes to Reynold number of 400. The pressure drop of silicon oil 50 simulation is 15 kPa compared to reference of 27 kPa. Then, the pressure drop of silicon oil 500 simulation is 15.7 kPa compared to reference of 26 kPa. These results were presented in figure 4.1 and figure 4.2.

Table 4.1 Tabulation of the pressure drop across mixer

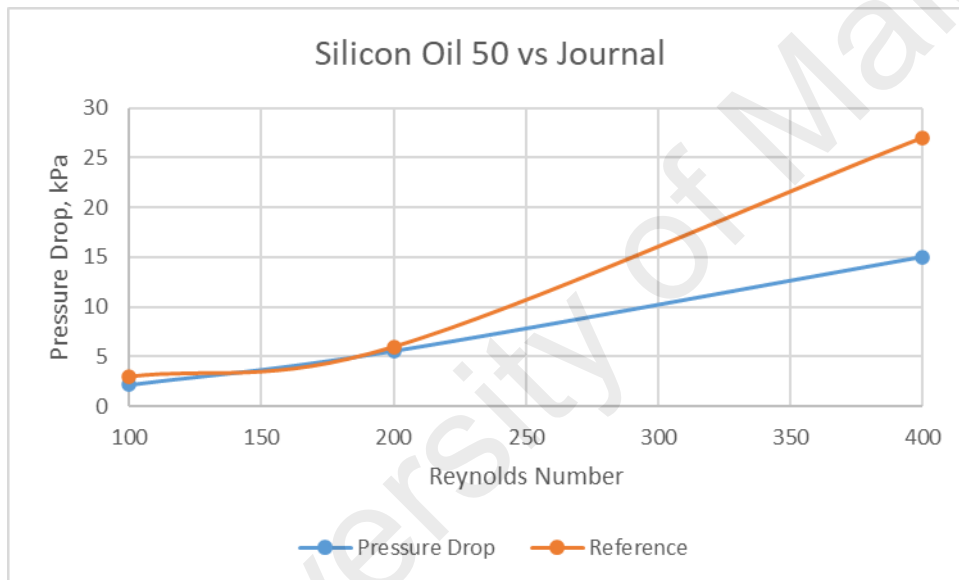| Re	Silicon Oil 50				Silicon Oil 500			
	P1 (Pa)	P2 (Pa)	ΔP (kPa)	$\Delta P *$ (kPa)	P1 (Pa)	P2 (Pa)	ΔP (kPa)	$\Delta P *$ (kPa)
100	2231.50	54.361	2.177	~3	2359.53	57.66	2.301	~2.5
200	5734.69	138.21	5.596	~6	6071.63	145.23	5.926	~6.2
400	15424.59	372.50	15.052	~27	16094.29	389.61	15.704	~26

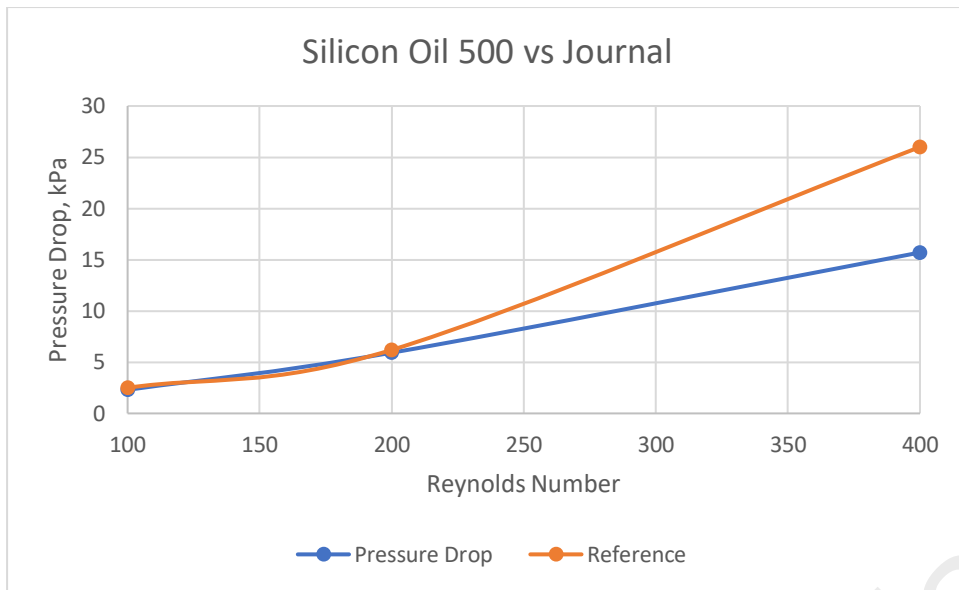Figure 4.1 The pressure drop comparison of silicon oil 50 case with the journal (Z.Jaworski, 2002)

Figure 4.2 The pressure drop comparison of silicon oil 500 case with the journal
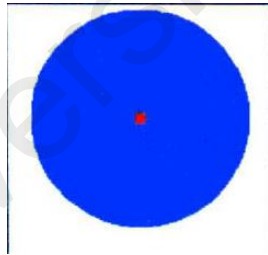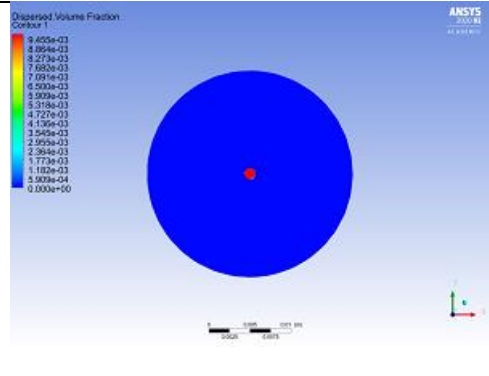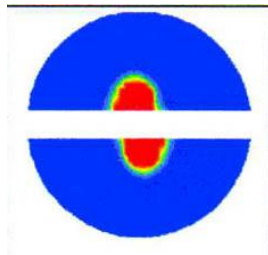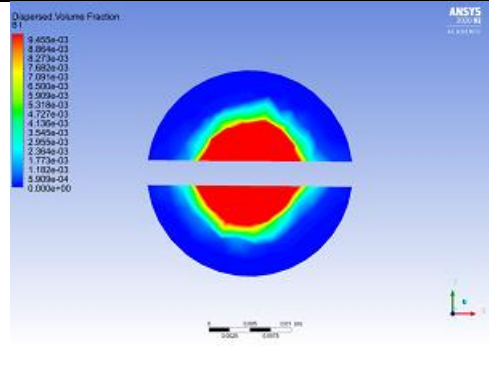
Mixing efficiency

The area-weighted uniformity index of volume fraction (dispersed phase) shows that silicon oil 50 and silicon oil 500 becomes more and more dispersed into continuous phase as it moves through each blade. Table 4.2 shows the area-weighted uniformity index (volume fraction of dispersed phase) across each blade. The value 0 represents no mixing of dispersed phase and continuous phase and the value 1 indicates that both phases has fully mixed. The inlet has a uniformity index of 0.00162 which shows the least mixing and it increases to 0.90607 after V insert. However, the outlet of silicon oil 50 shows a lower uniformity index compared to silicon oil 500. This could be caused by settling back of silicon oil 50 at the outlet due to low viscosity compared to silicon oil 500.
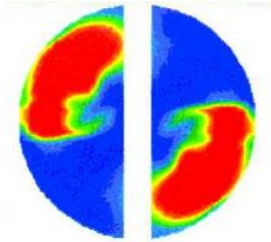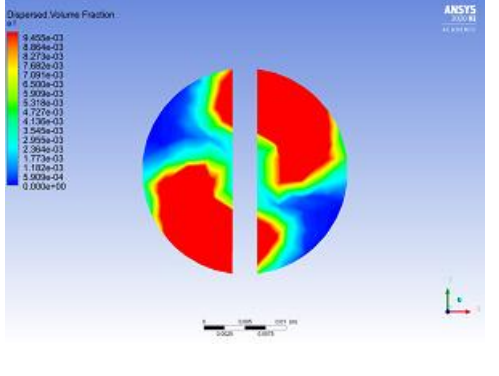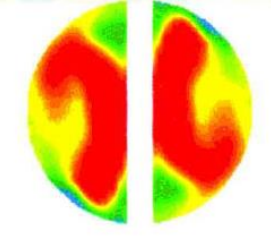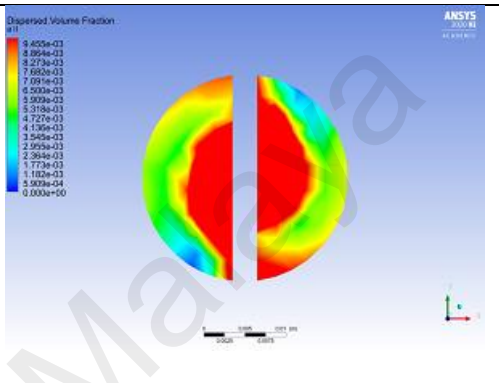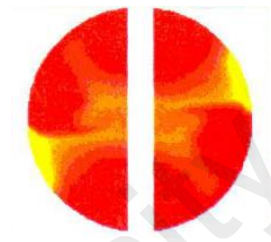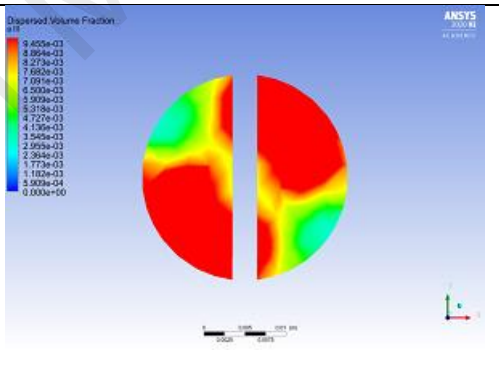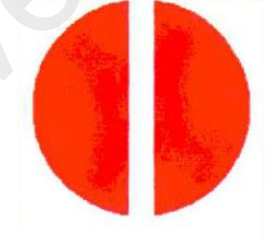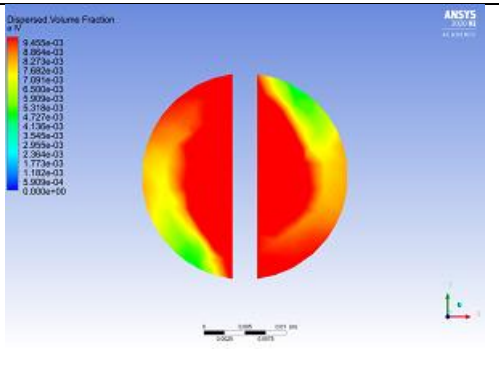
Table 4.2 The area weighted uniformity index of dispersed phase volume fraction for silicon oil 50 and silicon oil 500 (Reynolds Number 400)

Area	Uniformity Index – Area Weighted (Silicon Oil 50)	Uniformity Index – Area Weighted (Silicon Oil 500)
Inlet	0.00162	0.00162
Before I Insert	0.26730	0.26748
After I Insert	0.56269	0.56304
After II Insert	0.69464	0.69937
After III Insert	0.79145	0.79328
After IV Insert	0.86786	0.87021
After V Insert	0.90607	0.90714
Outlet	0.65270	0.98072

From table 4.2 it can be seen that both simulation and reference paper has good agreement even though not exactly same pattern. The range of local volume fraction used was 0 to 0.00975 which has been taken from the reference journal. At inlet, both the pattern are same since the flow just started. Before I insert, the pattern is same but the simulation result is more dispersed compare to reference. After I insert, both the pattern are same but simulation results has taken small area of other region since its more dispersed. After III insert, we can still see the butterfly pattern on simulation although not as profound as reference. Starting from after III insert to after V insert, we can see that reference has slightly better dispersion of silicon oil 50.

Table 4.3 Comparison of local dispersed phase volume fraction between simulation and reference journal.

Z(m)	Reference ((Z.Jaworski, 2002)	Simulation Result
0 (Inlet)		
0.07 (Before I insert)		

0.1075 (After I insert)		
0.145 (After II insert)		
0.1825 (After III insert		
0.22 (After IV insert)		

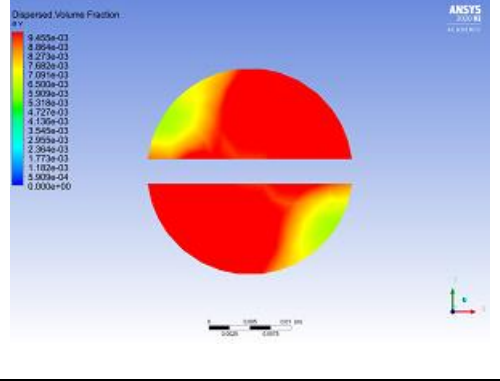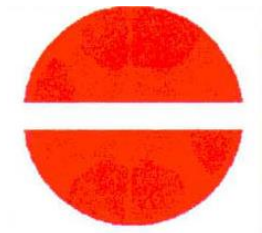| 0.2575 (After V insert)		

4.2 The Blade Twist Angle

From table 4.3, more complicated the twist more pressure drop happens. The 180-degree blade has a pressure drop of 16139 pa while the 90 degree blade has the lowest pressure drop of 9916 pa. The 180-degree blade has more curved surface which restricts the flow and gives higher frictional loss to the fluid. Thus, there is higher pressure drop.

Table 4.4 Pressure drop comparison between blade twist angle of 180^0, 150^0, 120^0 and 90^0.

Blade twist angle	P1 (Pa)	P2 (Pa)	ΔP (Pa)
180^0	15424.59	372.56	15052.03
150^0	11777.32	378.63	11398.69
120^0	11724.06	341.11	11382.95
90^0	10129.51	362.69	9766.82

The area weighted uniformity index is used to quantify the mixing performance of the static mixer with different blade twist angle. The 150^0 and 90^0 blade twist angle had better mixing performance compared to 180^0 blade. This could be seen from figure 4.3 where the uniformity index for 150^0 and 90^0 blade twist angle is above the 180^0 blade. But, 120^0 blade twist angle shows lower mixing performance compared to 180^0 blade as shown in figure 4.3. When both pressure drop and mixing performance is accounted, the 90^0 blade twist angle outperform other blade twist angle.

Table 4.5 The area weighted uniformity index of dispersed phase volume fraction for blade twist angle 180^0, 150^0, 120^0 and 90^0.

Area	Uniformity Index – Area Weighted			
	(180^0 twist angle)	(150^0 twist angle)	(120^0 twist angle)	(90^0 twist angle)
Inlet	0.00162	0.00160	0.00160	0.00160
Before I Insert	0.26730	0.39495	0.28735	0.38908
After I Insert	0.56269	0.66054	0.49012	0.63224
After II Insert	0.69464	0.79441	0.67086	0.75031
After III Insert	0.79145	0.86410	0.75704	0.83791
After IV Insert	0.86786	0.93492	0.83849	0.90025
After V Insert	0.90607	0.94752	0.86988	0.93757
Outlet	0.65270	0.97939	0.88292	0.98651
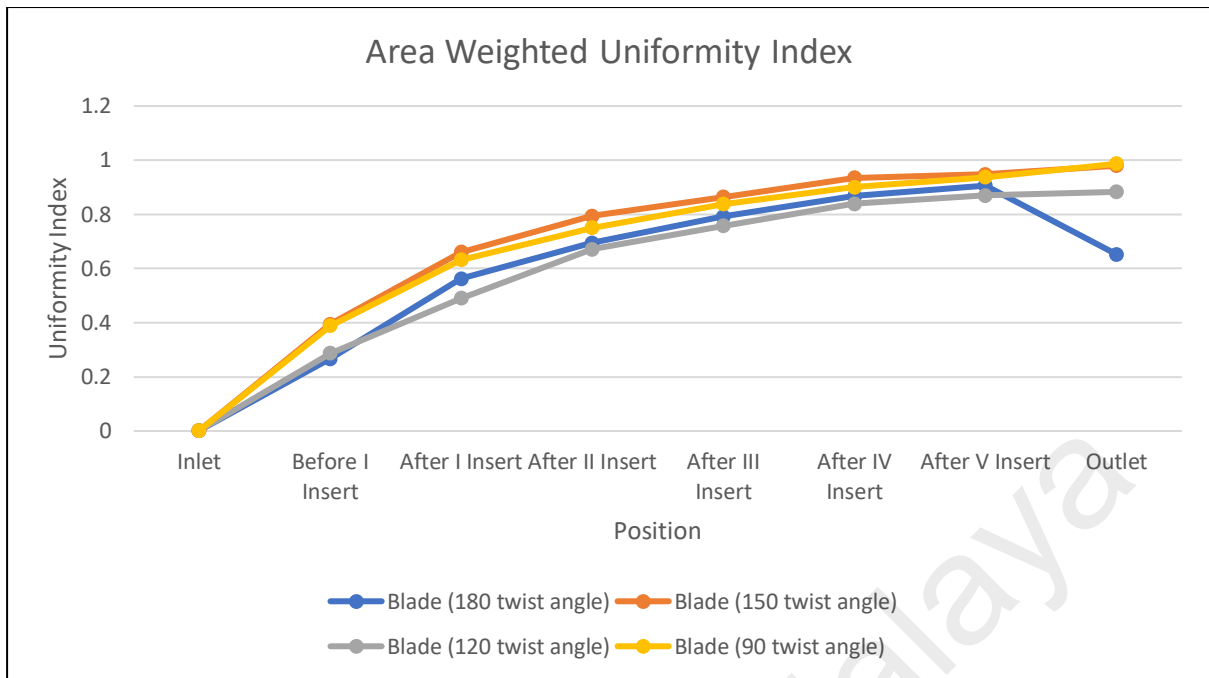
Figure 4.3 The area weighted uniformity index of dispersed phase volume fraction for blade twist angle 180^0, 150^0, 120^0 and 90^0

The table 4.6 compares the mixing performance of 90-degree blade with 180-degree blade. At the end of Z=0.2575, the 90-degree blade shows better mixing performance compared to 180-degree blade. Even during the initial blades, the 90-degree blade shows better mixing. This maybe due to lower pressure at initial steps of 90-degree blade. Hence, a 90-degree blade exhibit better performance in terms of pressure drop and mixing characteristics.

Table 4.6 illustration of mixing performance of Blade 180-degree (more twist) with Blade 90-degree (less twist).

Z(m)	Blade 90-degree	Blade 180-degree
0 (Inlet)		
0.07 (Before I insert)		
0.1075 (After I insert)		
0.145 (After II insert)		

0.1825 (After III insert		
0.22 (After IV insert)		
0.2575 (After V insert)		
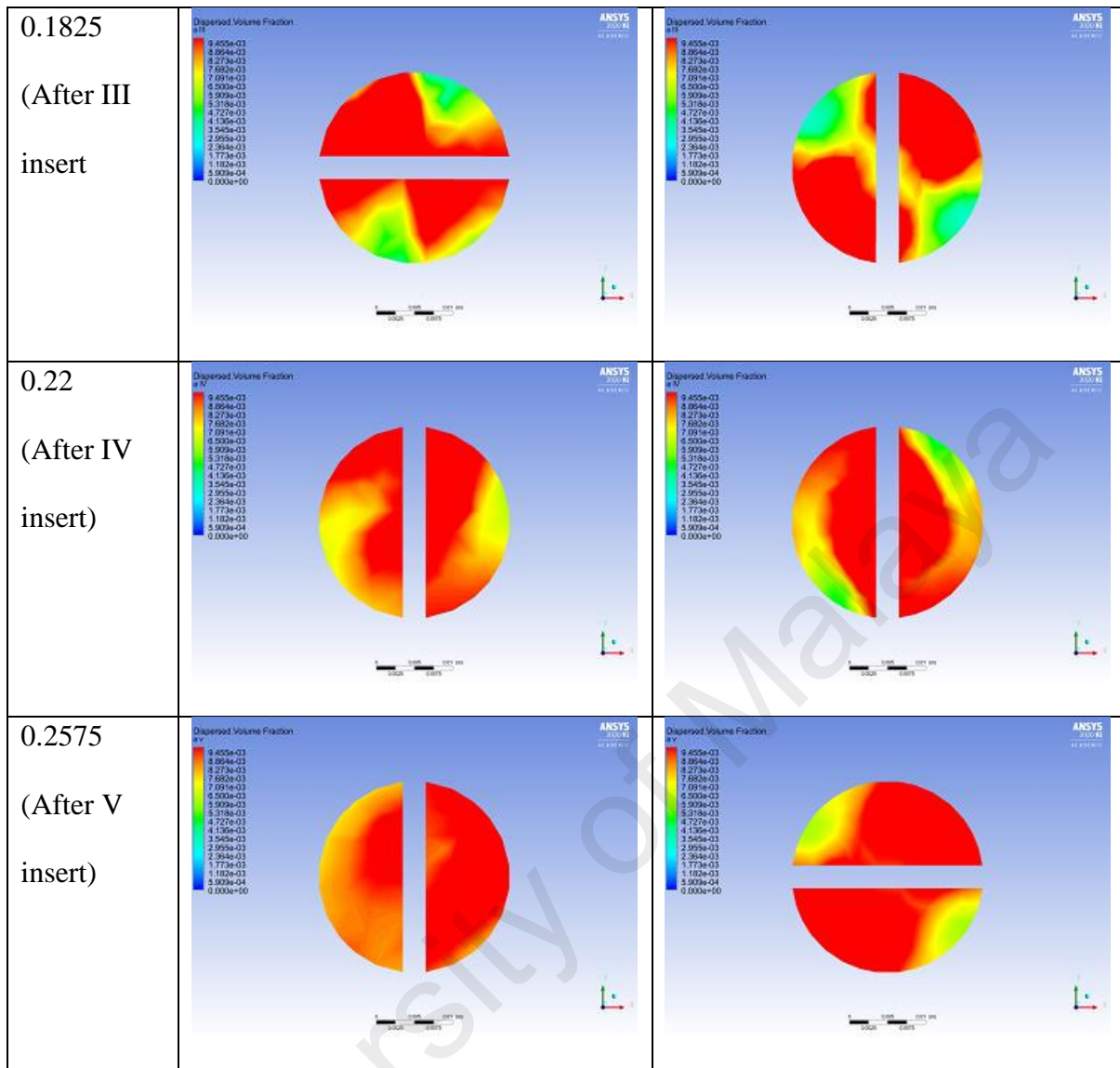
4.3 The Blade Length

The table 4.7 compare pressure drop when different length of blade were used. The blade do not have significant important on the pressure drop of fluid flow. But the exit pressure of blade 45mm is negative which can obstruct the flow. So, increasing the length may increase the residence time of the flow and the flow may become unstable and obstruct.

Table 4.7 Pressure drop comparison between blade length 30mm, 33.75mm, 37.5mm, 41.25mm and 45mm.

Blade Length (mm)	P1 (Pa)	P2 (Pa)	ΔP (Pa)
30	15971.46	791.37	15180.09
33.75	15118.37	604.98	14513.39
37.5	15424.59	372.56	15052.03
41.25	14462.28	139.12	14323.14
45	14784.38	3.9876	14780.39

Table 4.8 The area weighted uniformity index of dispersed phase volume fraction for blade length of 30mm, 33.75mm, 37.5mm, 41.25mm and 45mm.

Area	Uniformity Index – Area Weighted				
	30mm	33.75mm	37.5mm	41.25mm	45mm
Inlet	0.00156	0.00160	0.00162	0.00156	0.00156
Before I Insert	0.38003	0.38577	0.26730	0.38130	0.37344
After I Insert	0.69594	0.67827	0.56269	0.66287	0.66404
After II Insert	0.78941	0.79538	0.69464	0.79935	0.80918
After III Insert	0.85145	0.85705	0.79145	0.87317	0.88811

After IV Insert	0.91689	0.91279	0.86786	0.92519	0.94089
After V Insert	0.93990	0.94147	0.90607	0.95763	0.96984
Outlet	0.98909	0.99143	0.65270	0.93654	0.91433

Figure 4.4 The area weighted uniformity index of dispersed phase volume fraction for blade length of 30mm, 33.75mm, 37.5mm, 41.25mm and 45mm

Table 4.9 shows that the 30mm blade has better mixing performance than 37.5mm. On the last picture (z=0.2575), the 30mm blade has better distribution of silicon oil 50. This may be depending on the blade twist angle. The 37.5mm blade may perform better with other blade twisting angle.

Table 4.9 illustration of mixing performance of Blade 30mm (shorter) with Blade 37.5mm (longer).

Z(m)	Blade 30mm	Blade 37.5mm
0 (Inlet)		
0.07 (Before I insert)		
0.1075 (After I insert)		
0.145 (After II insert)		

0.1825 (After III insert		
0.22 (After IV insert)		
0.2575 (After V insert)		
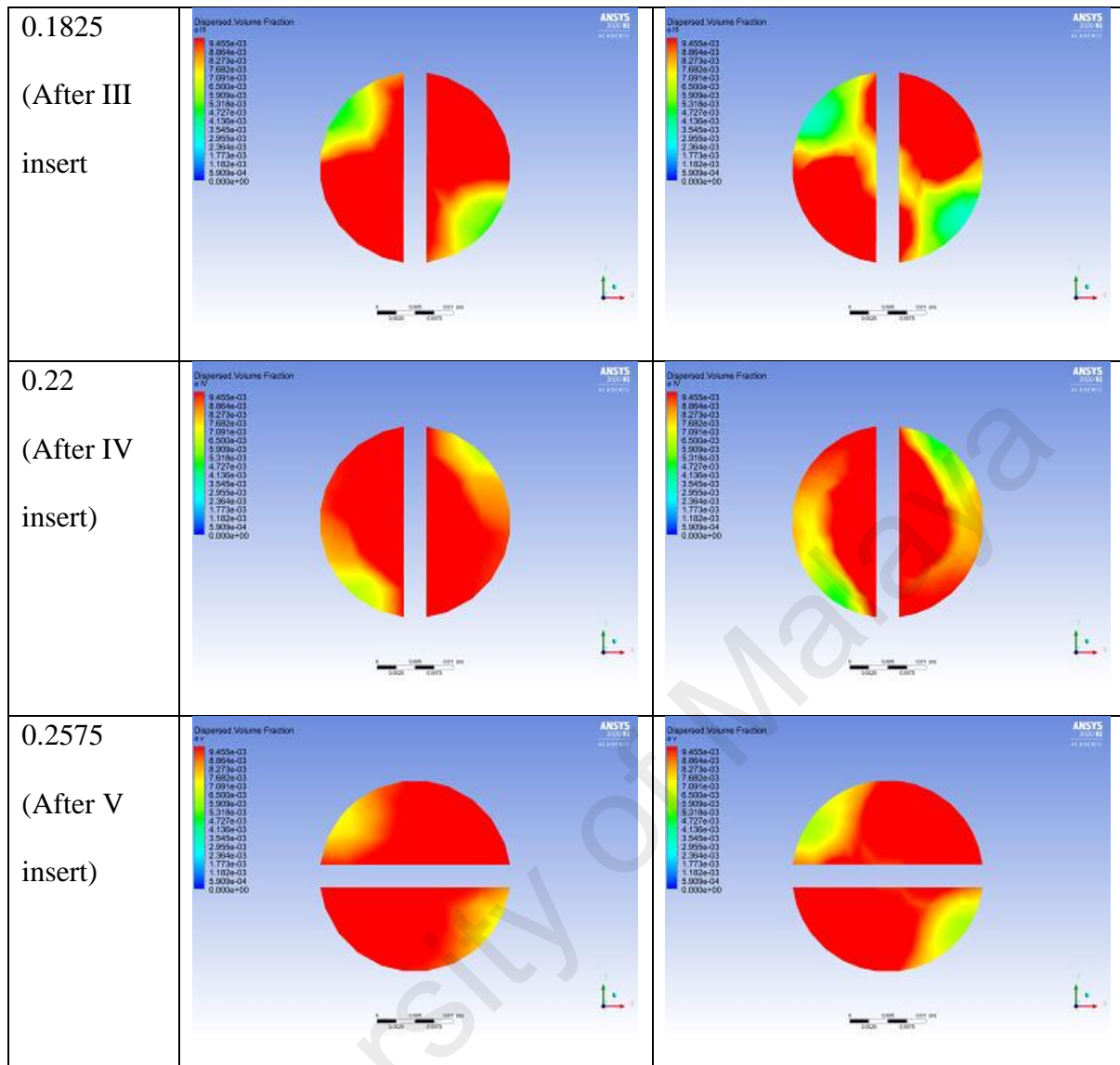
CHAPTER 5 CONCLUSION

In conclusion, the smaller the twist angle the better the performance in term of pressure drop and mixing performance. The 90-degree twist shows better mixing characteristics with low pressure drop compared to 180-degree twist blade. The 120-degree and 150-degree twist angle also better than the 180-degree twist. However, the configuration must always remain clockwise and anti-clockwise between the mixer blades. The blade length does not show a sounding effect on the pressure drop and mixing performance in the static mixer.

However, further studies should be conducted to determine the right twist angle to the right blade length. The blade twist angle and blade length dependent on each other for producing a good mixing performance. Future studies should extend on balancing this two aspects of the static mixer in achieving the optimum fluid mixing.

References

Akram Ghanem, T. L. (2014). Static mixers: Mechanisms, applications, and characterization methods-A review. *Chemical Engineering Research and Design*, 205-228.

Aubin, J. F. (2005). Design of micromixersusing CFD modeling. *Chemical Engineering Science 60*, 2503-2516.

Huibo Meng, G. Z. (2016). The effect of symmetrical perforated holes on the turbulent heat transferin the static mixer with modified Kenics segments. *International Journal of Heat and Mass Transfer*, 647-659.

Hyun-Seob Song, S. P. (2005). A general correlation for pressure drop in a Kenics static mixer. *Chemical Engineering Science 60*, 5696-5704.

Lynn, R. (1958). Turbulator. *US Patent 2,852,042, assigned to TheGarrett Corporation.*

M.J.Bakker. (1949). Dispositif pour préparer du béton ou unematière analogue. *French Patent*, 959,155.

M.M. Haddadi, S. D. (2020). CFD modeling of immiscible liquids turbulent dispersion in Kenics static mixers: Focusing on droplet behavior. *Chinese Journal of Chemical Engineering*, 348-361.

Pedro F. Lisboa, J. F. (2010). Computational-fluid-dynamics study of a Kenics static mixer as a heat exchangerfor supercritical carbon dioxide. *The Journal of Supercritical Fluids*, 107-115.

Petrole, L. C. (1931). Dispositif pour le mélangede deux ou plusieurs fluides. *French Patent*, 735,033.

S. J. Chen, D. L. (1978). Gas-liquid and liquid-liquid dispersions in a Kenics Mixer. *Paper presented at the 71 st Annual AlChe Meeting*.

Sutherland, W. (1784). Improvement in apparatus for preparing gaseous fuel. *UK Patent*.

Thakur, R. V. (2003). Static mixers in the process industries – a review. *ICheme 81*, 787-826.

Vimal Kumar, V. S. (2008). Performance of Kenics static mixer over a wide range of Reynolds number. *Chemical Engineering Journal 139*, 284-295.

Z.Anxionnaz, M. C. (2008). Heat exchanger/reactor (HEX reactors): concepts, technologies: state-of-the-art. *Chemical Engineering*, 2029-2050.

Z.Jaworski, P.-O. (2002). Two-Phase Laminar Flow Simulations in a Kenics static Mixer. *Trans ICheme Vol 80*, 910-916.